Biomedicine & Pharmacotherapy 158 (2023) 114185

Contents lists available at ScienceDirect

Biomedicine & Pharmacotherapy

journal homepage: www.elsevier.com/locate/biopha

Gongolarones as antiamoeboid chemical scaffold

Rubén L. Rodríguez-Expósito [a,b,c,1], Desirée San Nicolás-Hernández [a,b,c,1], Ines Sifaoui [a,b,c], Cristina Cuadrado [d], Lizbeth Salazar-Villatoro [e], María Reyes-Batlle [a,b,c], Antonio Hernández-Daranas [d], Maritza Omaña-Molina [f], José J. Fernández [g,h,*], Ana R. Díaz-Marrero [d,g,*], José E. Piñero [a,b,c,i,**], Jacob Lorenzo-Morales [a,b,c,i,**]

[a] Instituto Universitario de Enfermedades Tropicales y Salud Pública de Canarias (IUETSPC), Universidad de La Laguna (ULL), Tenerife, Spain
[b] Departamento de Obstetricia y Ginecología, Pediatría, Medicina Preventiva y Salud Pública, Toxicología, Medicina Legal y Forense y Parasitología, Universidad de La Laguna, Tenerife, Spain
[c] Red de Investigación Cooperativa en Enfermedades Tropicales (RICET), Spain
[d] Instituto de Productos Naturales y Agrobiología (IPNA), Consejo Superior de Investigaciones Científicas (CSIC), Tenerife, Spain
[e] Departamento de Infectómica y Patogénesis Molecular, Centro de Investigación y de Estudios Avanzados del Instituto Politécnico Nacional, Ciudad de México, Mexico
[f] Facultad de Estudios Superiores Iztacala, Medicina, UNAM, Tlalnepantla, 54090, Estado de México, Mexico
[g] Instituto Universitario de Bio-Orgánica Antonio González (IUBO AG), Universidad de La Laguna (ULL), Tenerife, Spain
[h] Departamento de Química Orgánica, Universidad de La Laguna (ULL), Tenerife, Spain
[i] Consorcio Centro de Investigación Biomédica En Red (CIBER), Área de Enfermedades Infecciosas (CIBERINFEC), Instituto de Salud Carlos III, Madrid, Spain

ARTICLE INFO

Keywords:
Acanthamoeba spp.
Gongolarones
Meroterpenoid
Gongolaria abies-marina
Programmed cell death
Autophagy

ABSTRACT

Free Living Amoeba (FLA) infections caused by *Acanthamoeba* genus include chronic nervous system diseases such as Granulomatous Amoebic Encephalitis (GAE), or a severe eye infection known as *Acanthamoeba* keratitis (AK). Current studies focused on therapy against these diseases are aiming to find novel compounds with amoebicidal activity and low toxicity to human tissues. Brown algae, such as *Gongolaria abies-marina* (previously known as *Cystoseira abies-marina,* S.G. Gmelin), presents bioactive molecules of interest, including some with antiprotozoal activity. In this study, six meroterpenoids were isolated and purified from the species *Gongolaria abies-marina.* Gongolarones A (**1**), B (**2**) and C (**3**) were identified as new compounds. Additionally, cystomexicone B (**4**), 1′-methoxyamentadione (**5**) and 6*Z*-1′-methoxyamentadione (**6**) were isolated. All compounds exhibited amoebicidal activity against *Acanthamoeba castellanii* Neff, *A. polyphaga* and *A. griffini* strains. Gongolarones A (**1**) and C (**3**) showed the lowest IC_{50} values against the two stages of these amoebae (trophozoite and cyst). Structure-activity relationship revealed that the cyclization by ether formation from C-12 to C-15 of **1**, and the isomerization $\Delta^{2\,t}$ to $\Delta^{3\,t}$ of **3**, increased the antiamoeboid activity of both compounds. Furthermore, gongolarones A (**1**) and C (**3**) triggered chromatin condensation, mitochondrial malfunction, oxidative stress, and disorganization of the tubulin-actin cytoskeleton in treated trophozoites. Moreover, transmission electron microscopy (TEM) images analysis revealed that compounds **1** and **3** induced autophagy process and inhibited the encystation process. All those results suggest that both compounds could induce programmed cell death (PCD) in *Acanthamoeba.*

1. Introduction

Neglected Tropical Diseases (NTDs) are defined by the World Health Organization as infections occurring in tropical and sub-topicals regions. They are designed by neglected as they occur in the poorest populations often living in remote rural or peri-urban areas in developing countries [1]. Those infections could be caused by viruses, bacteria, fungi, helminthic parasites and/or protozoa. Additionally, to the high spread of

* Corresponding authors at: Instituto Universitario de Bio-Orgánica Antonio González (IUBO AG), Universidad de La Laguna (ULL), Tenerife, Spain.
** Corresponding authors at: Instituto Universitario de Enfermedades Tropicales y Salud Pública de Canarias (IUETSPC), Universidad de La Laguna (ULL), Tenerife, Spain.
E-mail addresses: jjfercas@ull.edu.es (J.J. Fernández), adiazmar@ull.edu.es (A.R. Díaz-Marrero), jpinero@ull.edu.es (J.E. Piñero), jmlorenz@ull.edu.es (J. Lorenzo-Morales).
[1] These authors contributed equally: Rubén L. Rodríguez- Expósito and Desirée San Nicolás-Hernández.

https://doi.org/10.1016/j.biopha.2022.114185
Received 15 November 2022; Received in revised form 23 December 2022; Accepted 28 December 2022
Available online 9 January 2023

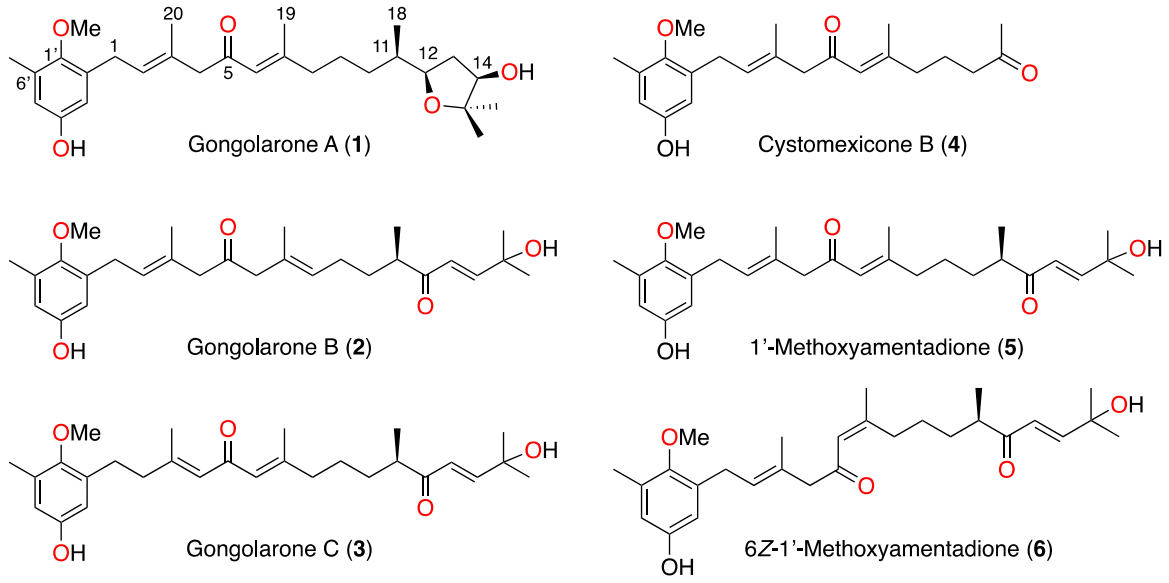

Fig. 1. Meroterpenoids isolated from the brown algae *Gongolaria abies-marina*.

those diseases, the incidence of Emerging and Re-Emerging Infectious Diseases especially from parasites have increased in recent years. This group includes the expansion of an infection to a new area or population and the increase of an existing infection in a specific area [2,3].

Free Living Amoeba (FLA) infections are recognized as emerging and re-emerging diseases. These protozoan parasites are ubiquitous and have been isolated from environmental habitats such as water, air, soil, among others and from clinical samples [4,5]. Even though, most FLA are non-pathogenic, some species of *Acanthamoeba* genus, and the species *Balamuthia mandrillaris, Naegleria fowleri* and *Sappinia diploidea,* were found to be pathogenic to human and other animals [6].

Acanthamoeba genus is the most isolated FLA from both clinical and environment samples. Moreover, it is responsible of granulomatous amoebic encephalitis (GAE) and a severe corneal infection, *Acanthamoeba* keratitis (AK), that can cause blindness [7,8]. Recently, the incidence of AK cases has shown a remarkable increase worldwide which is mainly related to the increase of contact lens wearers [9]. In addition, the treatment of these infections has been undermined by resistance, variable efficacy between strains or species, toxicity, parenteral administration, requirement for long courses of administration and adverse effects and cost [10,11].

The application of molecules produced by marine organisms to treat several diseases has notably increased in the recent years [12]. Among these organisms, macroalgae contains a wide variety of bioactive secondary metabolites including phlorotannins, glycerols, quinones, polyketides, polysaccharide, diterpenoids, phenolic compounds, sterols, cyclic peptide, lipids, and alkaloids [13,14]. Lately, several reports have confirmed the diverse pharmacological properties of seaweeds as antimicrobial, anti-helminthic, cytotoxic, anti-inflammatory, and antiprotozoal among other biological activities [15–17].

Cystoseira abies-marina (S.G. Gmelin), previously named *Treptacantha abies-marina* (S.G. Gmelin), has been recently renamed as *Gongolaria abies-marina* (S. G. Gmelin) [18,19]. This species of marine macro-algae is a canopy-forming brown seaweed distributed throughout the Mediterranean, the Macaronesian Region, and the coast of Africa [20]. In the Canary Islands, this alga has been reported from all over the archipelago, being particularly abundant in the intertidal zone [21]. Barreto *et al.*, (2012) evaluated the antioxidant and antiproliferative activities of different organic extracts of *Cystoseira abies-marina*. The dichloromethane extract was endowed with a specific antiproliferative activity towards Hela cells by inducing apoptosis [22]. Likewise, certain molecules isolated from this seaweed have been reported by their antioxidant, cytotoxic, anti-inflammatory, and antifungal bioactivities [23–26]. However, despite the several chemical studies available of *Cystoseira* genus, there are only a few reports describing the antiprotozoal potential effects of its crude extracts. Among them, leishmanicidal, antimalarial and trypanosomicidal activities of isolated molecules from *Cystoseira* spp. extracts have been proved[27–31].

As part of an ongoing research on the isolation and characterization of amoebicidal molecules from marine macroalgae, the present work describes the bio-guided fractionation of the organic extracts of *Gongolaria abies-marina* and the isolation of three new metabolites, gongolarones A-C (**1**-**3**), together with cystomexicone B (**4**), 1′-methoxyamentadione (**5**) and the isomer 6*Z*-1′-methoxyamentadione (**6**) (Fig. 1). The anti-*Acanthamoeba* activity of the pure compounds was tested and the effect of different apoptosis-like features of the most active metabolites was studied including chromatin condensation, alteration of the actin and microtubules organization, and mitochondrial damage events.

2. Materials and methods

2.1. General chemical experimental procedures

NMR spectra were acquired on a Bruker AVANCE 500 MHz or 600 MHz (Bruker Biospin, Falländen, Switzerland) instrument spectrometer at 300 K) when required. Bruker AVANCE 600 MHz spectrometer is equipped with a 5 mm TCI inverse detection cryoprobe (Bruker Biospin, Falländen, Switzerland). Standard Bruker NMR pulse sequences were utilized. NMR spectra were obtained by dissolving samples in CDCl3 (99.9%). Optical rotations were measured in $CHCl_3$ on a PerkinElmer 241 polarimeter (Waltham, MA, USA) by using a Na lamp. IR spectra were recorded using an Agilent Cary 630 FTIR spectrometer (Agilent Technologies, Inc., USA) equipped with an ATR unit. HPLC (High performance liquid chromatography) separations were carried out with an Agilent 1260 Infinity Quaternary LC equipped with a Diode Array Detector (Waldbronn, Germany). Thin-layer chromatography (TLC) silica gel plates were used to monitor column chromatography, visualized by UV light (254 nm) and developed with cobalt chloride (2%) as spraying reagent. All reagents and solvents were commercially available and used as received.

Table 1
NMR spectroscopic data of gongolarones A-C (**1–3**) ($CDCl_3$, 300 K, 600 MHz).

Position	Gongolarone A (**1**)		Gongolarone B (**2**)		Gongolarone C (**3**)	
	δ_C, type	δ_H (*J* in Hz)	δ_C, type	δ_H (*J* in Hz)	δ_C*, type	δ_H, (*J* in Hz)
1′	150.1, C		149.7, C		149.7, C	
2′	134.9, C		133.6, C		131.9, C	
3′	114.1, CH	6.49 dd (3.1, 3.1)	113.3, CH	6.57 d (3.1)	114.4, CH	6.74 d (3.1)
4′	152. 2, C		152.8, C		152.4, C	
5′	115.6, CH	6.48 dd (3.1, 3.1)	115.8, CH	6.54 d (3.1)	115.8, CH	6.54 d (3.1)
6′	132.1, C		132.2, C		135.2, C	
1	28.3, CH_2	3.40 d (7.4)	27.5, CH_2	3.38, d (7.5)	28.4, CH_2	2.70, ddd (10.2, 5.9, 3.3)
2	128.1, CH	5.46 dd (7.4, 7.4)	128.1, CH	5.37 ddd (7.5, 7.5, 1.3)	35.2, CH_2	a: 2.86 m; b: 2.77 m
3	131.1, C		130.5, C		157.4, C	
4	56.1, CH	3.10 d (14.4) 3.08 d (14.4)	53.4, CH_2	3.20, s	126.5, CH	6.04 d (1.3)
5	200.2, C		208.7, C		190.8, C	
6	121.9, CH	6.13 s	46.3, CH_2	3.13 d (5.0)	126.2, CH	6.03 d (1.3)
7	159.7, C		129.2, C		158.2, C	
8	41.8, CH_2	2.10 m	129.0, CH	5.30 ddd (7.2, 7.2, 0.9)	33.6, CH_2	a: 2.62 m; b: 2.52 m
9	25.3, CH_2	1.40 m; 1.50 m	26.2, CH_2	1.93 dddd (13.9, 7.2, 7.2, 7.2)	25.6, CH_2	1.50 m
10	31.9, CH_2	1.02 m; 1.40 m	33.6, CH_2	a: 1.71 m; b: 1.51 m	33.3, CH_2	a: 1.85 m; b: 1.51 m
11	37.6, CH	1.60 m	44.5, CH	2.76 ddd (8.7, 6.8, 4.9)	44.3, CH	2.86 m
12	79.7, CH	3.79 ddd (7.5, 7.0, 6.0)	204.9, CH		205.6, CH	
13	37.4, CH_2	a: 2.32 ddd (13.5, 7.0, 6.6) b: 1.66 ddd (13.5, 7.5, 4.6)	124.5 CH	6.39 d (15.6)	124.3 CH	6.48 d (15.7)
14	78.2, CH	3.99 ddd (7.5, 6.6, 4.6)	152.6, CH	6.94 d (15.6)	152.9, CH	6.95 d (15.7)
15	82.5, C		71.7, C		71.3, C	
16	22.6, CH_3	1.36 s	29.1, CH_3	1.40 s	29.1, CH_3	1.35 s
17	25.5, CH_3	1.20 s	29.1, CH_3	1.40 s	29.1, CH_3	1.35 s
18	15.9, CH_3	0.91 d (6.7)	17.0, CH_3	1.08 d (6.8)	16.9, CH_3	1.11 d (6.9)
19	19.5, CH_3	2.12 s	24.6, CH_3	1.71 d (0.9)	25.5, CH_3	1.91 d (1.3)
20	16.5, CH_3	1.71 s	16.7, CH_3	1.68 d (1.3)	25.7, CH_3	1.86 d (1.3)
Me-6′	16.4, CH_3	2.24 s	16.3, CH_3	2.25 s	16.3, CH_3	2.24 s
OMe-1′	60.7, CH_3	3.68 s	60.5, CH_3	3.67 s	61.0, CH_3	3.69 s
OH-4′		5.98 s				

* 13 C Chemical shifts determined by HSQC and HMBC experiment

2.2. Biological material

Specimens of *Gongolaria abies-marina* [19] were collected off the intertidal zone of the coast of Bajamar, Tenerife, Canary Islands (28°33'15.5"N 16°20'51.7"W) in April 2019. The seaweed was transported to the laboratory in a cool box where it was cleaned, rinsed, and dried at 35 °C in the dark. The algae were identified as *Gongolaria abies-marina* by Dr. M. Sansón from the Department of Marine Botany of Universidad de La Laguna. A voucher specimen is deposited under the code 11042019–3 at this University.

2.3. Extraction and isolation

The dried and powdered algal material (233.4 g) was first extracted by maceration at room temperature in dichloromethane (DCM), followed by extraction in ethyl acetate (EtOAc). The solvents were renewed three times to maximize extraction. Then, the organic extracts were combined, filtered and evaporated in a rotatory evaporator at 40 °C to give 1.94 g of crude extract. Gel filtration chromatography in a Sephadex LH-20 column, eluted with *n*-hexane/DCM/methanol (7:2:1) afforded 6 fractions (F1-F6). An additional size-exclusion chromatography in Sephadex LH-20 of subfraction F6 (689 mg) eluted with *n*-hexane, DCM and methanol (3:1:1) gave fractions F6.1- F6.7. Fraction F6.4 (257.4 mg) was isocratically chromatographed in a mixture *n*-hexane/EtOAc (1:1) using a medium pressure system with a Lobar LiChroprep Si 60 (40–63 μm) column to obtain 6 fractions (F6.4.1- F6.4.6). An open silica gel column using a step gradient mixture from $CHCl_3$/EtOAc (4:1) to 100% EtOAc allowed fractionation of F6.4.3 (110 mg) to give a pure compound identified as cystomexicone B (**4**, 1.39 mg) [32], and an enriched fraction F6.4.3–5 (51.86 mg). HPLC purification of F6.4.3–5 (Phenomenex, Luna 5 μm Silica (2) column, 100 Å, 250 × 10 mm) with *n*-hexane/EtOAc isocratic 3:2 for 10 mins (1 mL/min), gradient to 100% EtOAc in 50 min (2 mL/min) and 100% EtOAc for 5 min (2 mL/min), allowed purification of the new compounds gongolarone A (**1**, 0.48 mg, 39.1 min), gongolarone B (**2**, 1.75 mg, 34.1 min), and gongolarone C **3** (0.17 mg, rt: 30.2 min), together with the known meroterpenes 1′-methoxyamentadione (**5**, 6.22 mg, 42.1 min) and 6*Z*-1′-methoxyamentadione (**6**, 3.10 mg, 37.1 min) [32].

1. Gongolarone A (**1**): Colorless oil; $[\alpha]_D^{20}$ − 7 (*c* 0.04, $CHCl_3$); IR ν_{max} 2926, 2855, 1684, 1040 cm^{-1}; HRESIMS *m/z* 481.2943 $[M+Na]^+$ (calc. $C_{28}H_{42}O_5Na$, 481.2930); ^1H and ^{13}C NMR, see Table 1.
2. Gongolarone B (**2**): Colorless oil; $[\alpha]_D^{20}$ − 22 (*c* 0.17, $CHCl_3$); IR ν_{max} 2970, 2929, 1699 cm^{-1}; HRESIMS *m/z* 479.2770 $[M+Na]^+$ (calc. $C_{28}H_{40}O_5Na$, 479.2773); ^1H and ^{13}C NMR, see Table 1.
3. Gongolarone C (**3**): Colorless oil; $[\alpha]_D^{20}$ − 14 (*c* 0.04, $CHCl_3$); IR ν_{max} 2926, 2851, 1685 cm^{-1}; HRESIMS *m/z* 479.2781 $[M+Na]^+$ (calc. $C_{28}H_{40}O_5Na$, 479.2773); ^1H and ^{13}C NMR, see Table 1.
4. Cystomexicone B (**4**): Colorless oil; ^1H and ^{13}C NMR spectra available at Supplementary Material. [32]
5. 1′-Methoxyamentadione (**5**): Colorless oil; $[\alpha]_D^{20}$ − 13 (*c* 0.09, $CHCl_3$); ^1H and ^{13}C NMR spectra available at Supplementary Material. [32]
6. 6*Z*-1′-Methoxyamentadione (**6**): Colorless oil; $[\alpha]_D^{20}$ − 34 (*c* 0.06, $CHCl_3$); ^1H and ^{13}C NMR spectra available at Supplementary Material. [32]

2.4. Computational molecular studies

All calculations were done following the general protocols described for DP4 + and J-DP4 [33–37]. In that sense, all possible stereoisomers were built and conformational searches done using the mixed torsional/low mode conformational sampling protocol in gas phase using the MMFF force field (as implemented in the Schrödinger 2021–1 suite of software, MacroModel Schrodinger release 2018–3; Schrodinger LLC: New York, 2018.). NMR calculations were undertaken using all

conformations within a 21 kJ/mol threshold of the lowest energy conformer found. DFT calculations were performed using Gaussian 09 [38]. DFT structure optimization of molecular mechanics structures were done at the B3LYP/6–31 G* level of theory. Magnetic shielding constants (σ) were calculated by means of the gauge including atomic orbitals (GIAO) method, [39] at the B3LYP/6–31 G* * or mPW1PW91/6–31 +G* * levels of theory as recommended for J-DP4 and DP4 + respectively. ^{1}H–^{1}H coupling constants used in the J-DP4 probability were calculated at the B3LYP/6–31 G* * level using only the Fermi contact term contribution. Unscaled chemical shifts (δ_u) were calculated using TMS as reference standard according to the following expression $\delta_u = \sigma_0 - \sigma_x$, where σ_x is the Boltzmann averaged shielding tensor (over all significantly populated conformations) and σ_0 is the shielding tensor of TMS computed at the same level of theory used to calculate σ_x. Boltzmann averaging was done according to Eq. 1:

$$\sigma^x = \frac{\sum_i \sigma_i^x e^{(-E_i/RT)}}{\sum_i e^{(-E_i/RT)}} \quad (1)$$

where σ_i^x is the shielding constant for nucleus x in conformer *i*, R is the molar gas constant (8.3145 J K^{-1} mol^{-1}), T is the temperature used for the calculation (298 K), and E_i is the relative energy of conformer *i* (to the lowest energy conformer) obtained from a single-point NMR calculation at the corresponding level of theory. The scaled chemical shifts (δ_s) were computed as $\delta_s = (\delta_u -$ (ere computed as shifts (rmer) obtained from a single-point NMR calculation at the corresponding level of theory. ntact teδ_u against δ_{exp}.

2.5. *Acanthamoeba spp. tested strains*

The antiamoebic effect of the three isolated meroterpenes gongolarones A (**1**), C (**3**), and cystomexicone B (**4**) was evaluated against three strains of *Acanthamoeba*: *Acanthamoeba castellanii* Neff, genotype T4 (ATCC 30010), *Acanthamoeba polyphaga*, genotype T4 (ATCC 30461) and *Acanthamoeba griffini*, genotype T3 obtained in a previous study [40]. *Acanthamoeba* strains were grown axenically in Peptone Yeast Glucose (PYG) medium (0.75% (w/v) proteose peptone, 0.75% (w/v) yeast extract, and 1.5% (w/v) glucose) containing 40 μg of gentamicin mL^{-1} (Biowest, Nuaillé, France).

2.6. *In vitro effect against the trophozoite stage of Acanthamoeba spp*

The amoebicidal activity of meroterpenes gongolarones A (**1**), C (**3**), and cystomexicone B (**4**) against the trophozoite stage of *Acanthamoeba* strains was determined *in vitro* using the alamarBlue® method previously described [41]. *Acanthamoeba* spp. trophozoites were culture on a 96-well microtiter plates (50 μL from a stock solution of $5{\cdot}10^4$ cells/mL). After trophozoites attachment, 50 μL of serial dilutions of each molecule were added to each well. Finally, alamarBlue® Reagent (Life Technologies, Madrid, Spain) was placed into each well at an amount equal to 10% of the final volume and the plates were incubated during 96 h at 26 °C with a soft agitation. The plates were analysed using an EnSpire® Multimode Plate Reader (Perkin Elmer, Madrid, Spain) using a test wavelength of 570 nm and a reference wavelength of 630 nm.

2.7. *In vitro effect against of Acanthamoeba spp. cysts*

The cysticidal activity was evaluated by the alamarBlue® assay at 168 h and confirmed visually by inverted microscopy. Cysts of the *Acanthamoeba* strains were obtained as it has been described before [42,43]. First, 50 μL of $5{\cdot}10^4$ cysts/mL, as final concentration of mature cysts of *Acanthamoeba* strains, were cultivated in PYG medium in triplicate on a 96-well plate with 50 μL of serial dilutions of meroterpenes gongolarones A (**1**), C (**3**), and cystomexicone B (**4**). *Acanthamoeba* spp. cysts incubated in PYG medium were used as negative control. After an incubation of 168 h at 26 °C, the plate was centrifuged at 3000 rpm for 10 min and the supernatant was removed. Then, 100 μL of fresh PYG medium were added to each assay well and the alamarBlue® Reagent was placed into each well at 10% and the plates were incubated 168 h at 26 °C. Finally, the plates were analysed using an EnSpire® Multimode Plate Reader as it was described above.

2.8. *Cytotoxicity assays*

The evaluation of the cytotoxicity of the tested molecules was carried out using the murine macrophage cell line J774A.1 (ATCC TIB-67). Macrophages were cultured in RPMI (Roswell Park Memorial Institute, 1640 medium) supplemented with 10% foetal bovine serum at 37 °C and 5% CO_2 atmosphere. The cytotoxic effect of the evaluated molecules was tested using the alamarBlue® method as described before described for *in vitro* effect against the trophozoite stage.

2.9. *Fluorescent staining of actin distribution*

For direct fluorescent staining, samples were treated first with the IC_{90} of gongolarones A (**1**) and C (**3**). After 24 h of incubation, cells were fixed with formaldehyde and deposit on precoated coverslip. Later, cells were treated with Triton (0.1%) for 30 min followed by phalloidin–tetramethylrhodamine B isothiocyanate (phalloidin-TRITC; Sigma-Aldrich, Madrid) for another 30 min at room temperature. Finally, cells were washed with PBS 1X. Then, cells were examined by Z-stack imaging with a 100x objective of EVOS™ FL Cell Imaging System M5000 (Life Technologies, EE. UU.) at $\lambda_{exc} = 540$ nm and $\lambda_{em} = 570$ nm.

2.10. *Immunofluorescence staining of intracellular tubulin of Acanthamoeba trophozoites*

The trophozoites of *Acanthamoeba* strains were incubated using the same method described for fluorescent staining of intracellular actin. Then, cells were treated with 5% BSA in PBS 1X/150 mM saccharose for 30 min and washed with glycine 100 mM in PBS 1X for 5 min. Later, the trophozoites were incubated with the first tubulin antibody 1:1000 for an hour at room temperature (Monoclonal Anti-α-Tubulin antibody produced in mouse, Sigma-Aldrich, Madrid). Next, cells were incubated with the second antibody with Alexa 594 1:500 for an hour at room temperature in darkness (Goat anti-Mouse IgG (H+L) Highly Cross – Adsorbed Secondary Antibody, Alexa Fluor Plus 594; Thermo Fisher Scientific, Rockford; USA). Finally, cells were washed with PBS 1X and a drop of mounting DAPI solution was added (4′,6-Diamidino-2-phenylindole dihydrochloride; Sigma-Aldrich; Madrid). The trophozoites were examined by Z-stack imaging using an inverted confocal microscope Leica DMI 4000 B with a 63x objective (Leica Microsystems, Germany).

2.11. *Analysis of mitochondrial membrane potential*

The collapse of an electrochemical gradient across the mitochondrial membrane during apoptosis was detected with the JC-1 mitochondrial membrane potential detection kit (Cayman Chemicals, Vitro SA, Madrid, Spain). Trophozoites were cultured on 96-well plate at a final concentration of 10^5 cells/mL with PYG medium, treated with IC_{90} of the tested meroterpenes for 24 h and incubated with JC-1 reagent following the manufacturer's instructions. Images were taken on EVOS™ FL Cell Imaging System M5000 (Life Technologies, EE. UU.). The staining pattern allows the identification of two groups in a cellular population: live cells will show red fluorescence; and cells with low mitochondrial potential will show a higher level of green and red fluorescence, exhibiting a programmed cell dead (PCD). The images (40x magnification) obtained were processed using FIJI software (*Fiji is Just* ImageJ 1.53 q, National Institute of Health, USA), determining the mean values of red and green fluorescence intensity for each assay. All experiment were performed in triplicate.

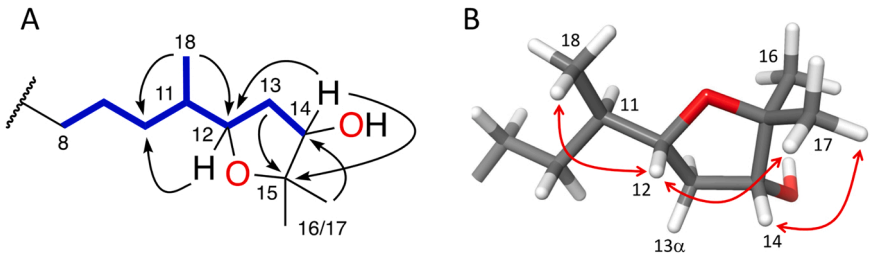

Fig. 2. (A) Selected COSY (blue) and HMBC correlations (arrows), and (B) key-NOE correlations of **1**.

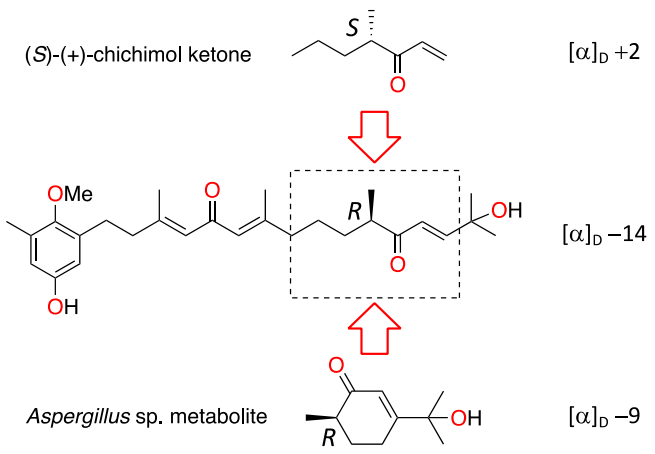

Fig. 3. Comparison of the common structural features and specific rotation of gongolarone C (**3**), (*S*)-(+)-chichimol ketone and metabolite from *Aspergillus* sp.

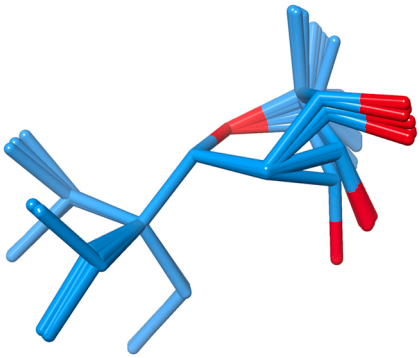

Fig. 4. Conformational ensemble of the C9-C18 moiety of gongolarone A (Fragment F1) including structures contributing more than 5% in the calculated Boltzmann populations. The experimental $^{3}J_{HH}$ values are consistent with the conformational freedom depicted.

2.12. Measurement of ATP

The ATP level was measured using a CellTiter-Glo Luminescent Cell Viability Assay (PROMEGA BIOTECH IBÉRICA S.L, Madrid, Spain). The effect of meroterpenes gongolarones A (**1**), C (**3**), and cystomexicone B (**4**) on the ATP production was evaluated by incubating 10^5 of cells/mL in PYG medium with the previously calculated IC_{90} for 24 h at 26 °C.

2.13. Double-stain assay for programmed cell death determination

A double-stain apoptosis detection kit (Hoechst 33342/PI) (Life Technologies, Madrid, Spain) and an EVOS™ FL Cell Imaging System M5000 (Life Technologies, EE. UU.) were used in this assay. The experiment was carried out by following the manufacturer's recommendations, and 10^5 cells/mL well were incubated for 24 h with the previously calculated IC_{90} of gongolarones A (**1**), C (**3**), and cystomexicone B (**4**). The double-staining pattern allows the identification of three groups in a cellular population: live cells will show only a low level of blue fluorescence, cells undergoing PCD will show a higher level of blue fluorescence (as chromatin condenses), and dead cells will show low-blue and high-red fluorescence (as the Propidium Iodide stain enters the nucleus). The images (40x) were analysed, and the values of mean blue and red fluorescence intensity were obtained with Fiji software (*Fiji is Just* ImageJ 1.53 q, National Institute of Health, USA).

2.14. Plasma membrane permeability

The SYTOX™ Green assay was performed to detect alterations on plasmatic membrane permeability in treated amoebae. First, 10^5

Table 3
In vitro Inhibition Concentration 90 (IC_{90}) value of tested meroterpenes against trophozoites of Acanthamoeba strains.

Compound	*A. castellanii* Neff IC_{90} (μM)	*A. polyphaga* IC_{90} (μM)	*A. griffini* IC_{90} (μM)
1	9.46 ± 0.79	16.17 ± 1.73	6.72 ± 0.55
3	13.33 ± 0.13	19.31 ± 1.93	8.24 ± 0.49
4	107.80 ± 8.02	241.46 ± 5.74	134.40 ± 9.48

Table 2
In vitro amoebicidal effect of meroterpenes **1–6** against trophozoites and cyst stages of different strains of *Acanthamoeba* spp., and their cytotoxicity effect against murine macrophages cell line J774A.1 (ATCC TIB-67). Chlorhexidine and voriconazole are the reference drugs used as positive control.

Compounds	*A. castellanii* Neff IC_{50} (μM)		*A. polyphaga* IC_{50} (μM)		*A. griffini* IC_{50} (μM)		J774A.1 CC_{50} (μM)
	Trophozoites	Cysts	Trophozoites	Cysts	Trophozoites	Cysts	
1	3.99 ± 0.14	10.44 ± 0.04	5.43 ± 0.30	14.85 ± 1.12	2.61 ± 0.16	11.09 ± 0.38	> 400
2	30.58 ± 3.78	-	47.59 ± 0.96	-	23.19 ± 3.98	-	25.62 ± 4.18
3	4.29 ± 0.08	10.64 ± 0.03	5.87 ± 0.03	6.85 ± 0.52	2.76 ± 0.11	10.05 ± 0.56	> 400
4	44.49 ± 1.05	41.03 ± 1.92	118.47 ± 9.16	> 200	51.44 ± 3.63	129.35 ± 0.36	> 400
5	24.03 ± 2.46	-	51.88 ± 0.23	-	21.52 ± 0.28	-	26.21 ± 2.26
6	26.11 ± 2.31	-	62.47 ± 7.55	-	28.79 ± 2.46	-	26.56 ± 4.03
Chlorhexidine	3.02 ± 0.89	5.97 ± 1.76	5.59 ± 0.04	9.41 ± 0.16	5.60 ± 0.07	7.38 ± 1.94	29.89 ± 0.19
Voriconazole	0.99 ± 0.04	3.45 ± 0.17	1.07 ± 0.02	6.98 ± 0.05	0.32 ± 0.01	0.92 ± 0.06	21.64 ± 2.20

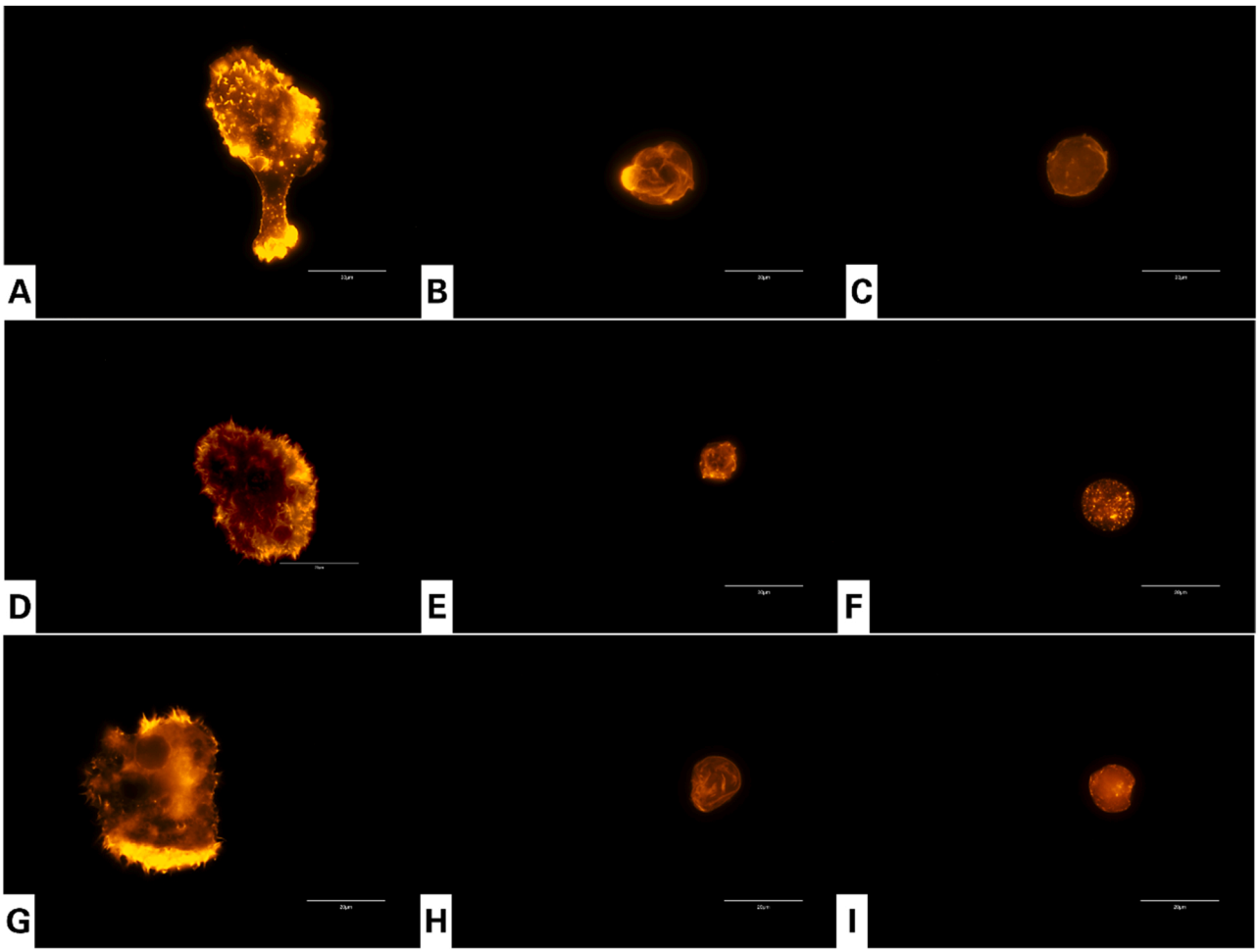

Fig. 5. Effect of IC_{90} of gongolarones A (**1**) (B, E, H) and C (**3**) (C, F, I) on trophozoites of *Acanthamoeba castellanii* Neff (A, B, C), *A. polyphaga* (D, E, F) and *A. griffini* (G, H, I) for 24 h. Control cells (A, D, G). The phalloidin-TRITC dye stain the actin cytoskeleton showing the networks organization with an orange fluorescence. All images (100x) are based on EVOS™ FL Cell Imaging System M5000 (Scale Bar 20 μm).

trophozoites were incubated with the previously calculated IC_{90} of each evaluated meroterpene. After 24 h of incubation, the SYTOX Green was added at a final concentration of 1 μM. The images were taken after 15 min of incubation in darkness with EVOS™ FL Cell Imaging System M5000 (Life Technologies, EE. UU.). All images (40x) obtained were processed using Fiji software for fluorescence quantification (*Fiji is Just* ImageJ 1.53 q, National Institute of Health, USA).

2.15. Intracellular ROS production using CellROX® Deep Red staining

The generation of intracellular reactive oxygen species (ROS) was assessed by using the CellROX® Deep Red fluorescent probe (Invitrogen, Termo Fisher Scientific, Madrid, Spain). The trophozoites were treated with the IC_{90} of each molecule for 24 h and exposed to CellROX® Deep Red (5 μM, 30 min) at 26 °C in the dark. Amoebae were observed in an EVOS™ FL Cell Imaging System M5000 (Life Technologies, EE. UU.). The images (40x) were analysed for fluorescence quantification using the method described above.

2.16. Transmission electron microscopy

The ultrastructure of *Acanthamoeba polyphaga* trophozoites were evaluated after an incubation with the IC_{90} of gongolarones A (**1**) and C (**3**) for 24 h. The samples were processed and prepared using the method previously reported [44,45]. Final sections obtained were observed in a JEOL JEM-1011 transmission electron microscope (JEOL Ltd. Tokyo, Japan).

2.17. Statistical analysis

All data are expressed as mean ± standard deviation. To highlight the effect of gongolarones A (**1**), C (**3**), and cystomexicone B (**4**) the fluorescence measure of different assay of *Acanthamoeba* spp. trophozoites were done, a statistical comparison was performed by a one-way analysis of variance (ANOVA), and a p-value (p) < 0.05 denoted the presence of a statistically significant difference. Statistical analyses were carried out using Sigma Plot 12.0 statistical analysis software (Systat Software) and GraphPad Prism 9.0. software programme (GraphPad Software, San Diego, CA, USA).

3. Results and discussion

3.1. Bioassay-guided isolation and identification of meroterpenes 1–6

Specimens of *Gongolaria abies-marina* were collected off the intertidal area of the Northeast coast of the island of Tenerife, Spain. Clean and dried algal material were powdered and sequentially extracted at room temperature with dichloromethane and ethyl acetate to afford an active crude extract against *Acanthamoeba* spp. (IC_{50} 53.2 ± 3.0 μg/mL against *A. castellanii* Neff). Gel filtration of the extract afforded an active fraction (F6) against the strains *A. castellanii* Neff (IC_{50} 36.1 ± 9.7 μg/mL), *A. polyphaga* (IC_{50} 86.1 ± 9.2 μg/mL), and *A. griffini* (IC_{50} 41.7

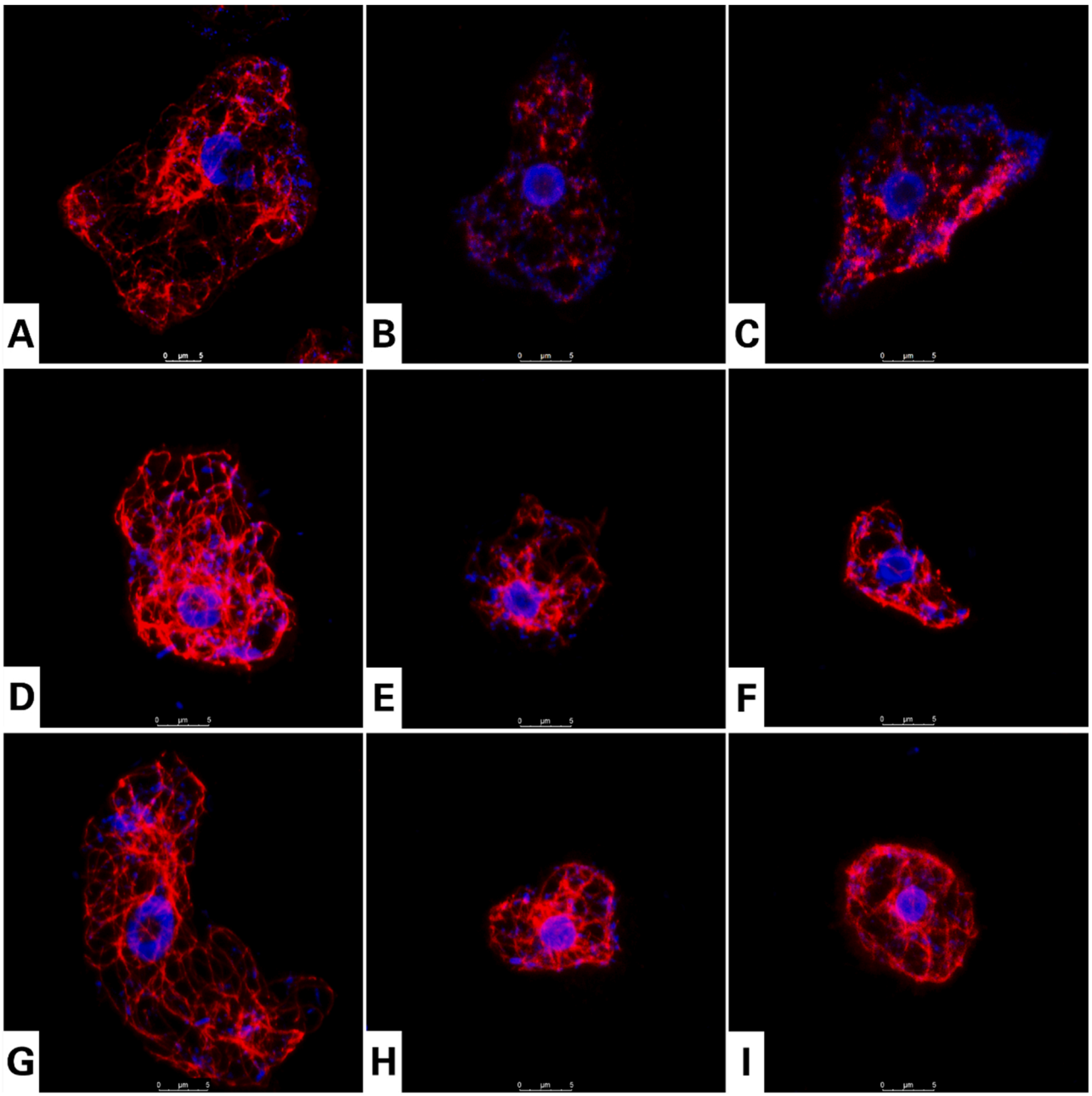

Fig. 6. Images (63x) of *Acanthamoeba castellanii* Neff (A, B, C), *A. polyphaga* (D, E, F) and *A. griffini* (G, H, I) incubated with IC_{90} of gongolarones A (**1**) (B, E, H) and C (**3**) (C, F, I) for 24 h. The tubulin antibodies stained the tubulin microtubules inside the cells, showing the intracellular organization emitting a red fluorescence. Tubulin microtubules demonstrated a normal conformation in control cells (A, D, G), whereas in the treated trophozoites the staining suggesting a disorganization or disruption of the tubulin microtubules (B, C, E, F, H, I). Mounting DAPI solution staining the acid nucleic of cells showing a blue fluorescence. The scale bar represents 5 μm. Images were obtaining using an inverted confocal microscope Leica DMI 4000 B (Scale Bar 5 μm).

± 3.2 μg/mL). After sequential bioassay-guided fractionation and purification of F6, three new compounds, gongolarones A-C (**1**-**3**), together with three known meroterpenoids **4**-**6** were obtained (Fig. 1). Their structures were determined based on extensive spectroscopic analysis, *in silico* calculations and comparison with data reported in the literature.

Gongolarone A (**1**) was obtained as an optically active, $[\alpha]_D^{20} - 7$ (*c* 0.04, $CHCl_3$), colorless oil. Its molecular formula $C_{28}H_{42}O_5$ was deduced from the sodium adduct $[M + Na]^+$ observed in the HRESIMS and indicated eight degrees of unsaturation. The ^1H NMR spectrum of **1** resemble that of the truncated meroterpenoid cystomexicone B (**4**) (Fig. S21, Supporting Material) and other analogues of the series [32, 46], which confirmed the presence of the characteristic signals of the toluhydroquinone nucleus linked to a terpenoid fragment: $\delta_{H\text{-}3'}$ 6.49 (dd, $J = 3.1, 3.1$ Hz, 1 H), $\delta_{H\text{-}5'}$ 6.48 (dd, $J = 3.1, 3.1$ Hz, 1 H), $\delta_{Me\text{-}6'}$ 2.24 (s, 3 H), $\delta_{OMe\text{-}1'}$ 3.68 (s, 3 H) (Table 1), accounting for four degrees of unsaturation. Additionally, two olefinic protons were identified at δ_H 6.13 (s, 1 H) and 5.46 (dd, $J = 7.4, 7.4$ Hz, 1 H), and a singlet at δ_H 5.98 for an interchangeable proton. The main differences observed were the presence of two multiplets of protons adjacent to heteroatom at δ_H 3.99 (ddd, $J = 7.5, 6.6, 4.6$ Hz, 1 H) and δ_H 3.79 (ddd, $J = 7.5, 7.0, 6.0$ Hz, 1 H), as well as two additional methyl groups compared to the three found in compound **4**, indicative of the diterpenic nature of the side chain of **1**. The analysis of the ^{13}C NMR spectrum confirmed 28 carbon atoms (Table 1), among them, one carbonyl resonance at $\delta_{C\text{-}5}$ 200.2 ppm, and 10 sp^2 signals between 160 and 114 ppm assigned to the

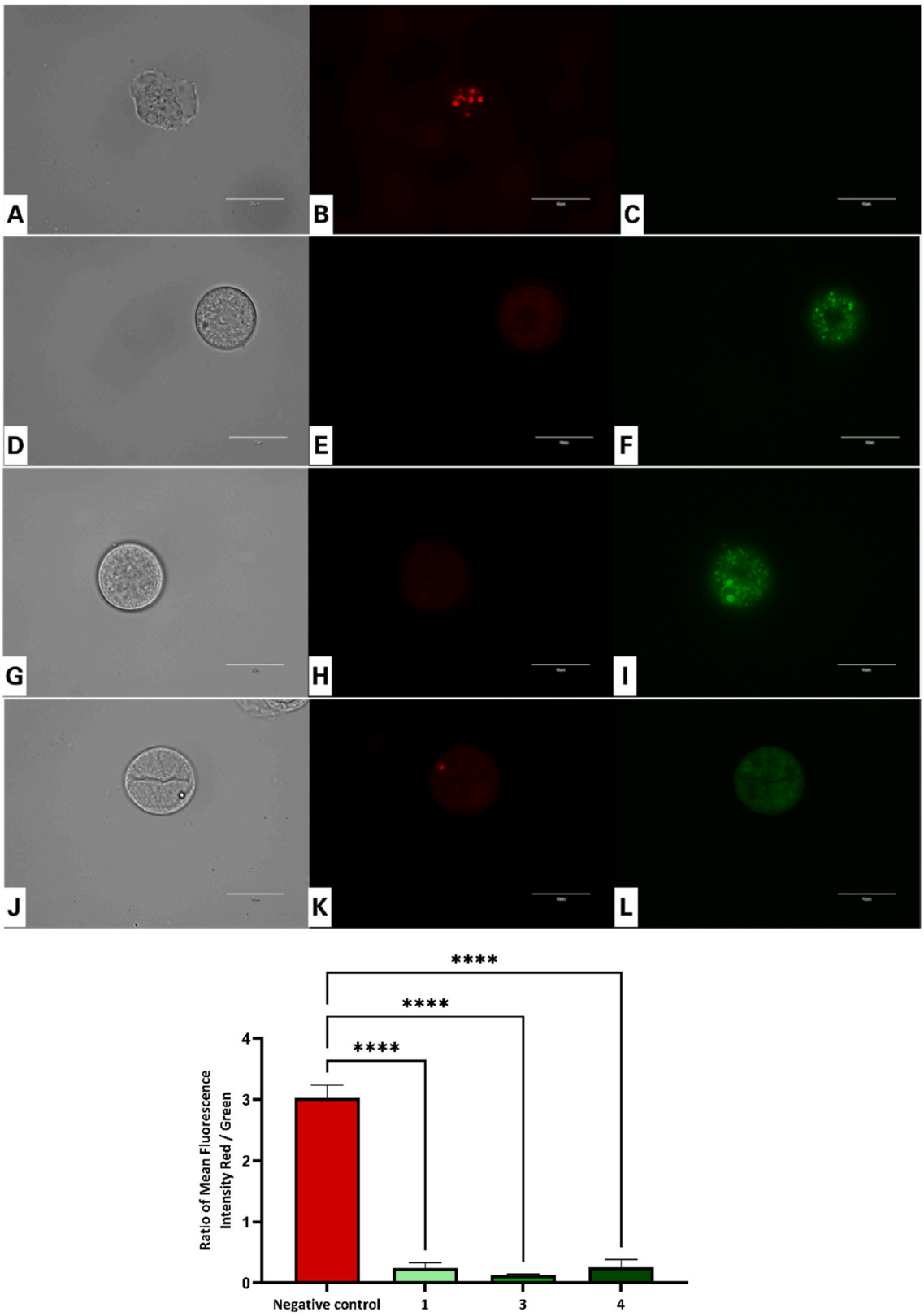

Fig. 7. *Acanthamoeba castellanii* Neff trophozoites incubated with the IC_{90} of gongolarones A (1) (D, E, F), C (3) (G, H, I) and cystomexicone B (4) (J, K, L) for 24 h. Due to collapse of the mitochondrial potential in treated cells, JC-1 dye accumulates in the cytoplasm in its monomeric form and emit green fluorescence (F, I, L). However, in healthy cells with a normal mitochondrial potential, JC-1 dye aggregates showed a red fluorescence (B). All images (100x) are based on EVOS™ FL Cell Imaging System M5000 (Scale Bar 20 μm). The graph includes the ratio between of the mean fluorescence emitted by the JC-1 stained cells. Differences between the values were assessed using One-Way Analysis of Variance (ANOVA). Data are presented as means ± SD, * ** * $p < 0.0001$; the results showed significant differences when comparing treated cells to negative control. Mean fluorescence intensity of stained cells for each assay were determined using Fiji Software. All the experiments were conducted in triplicate.

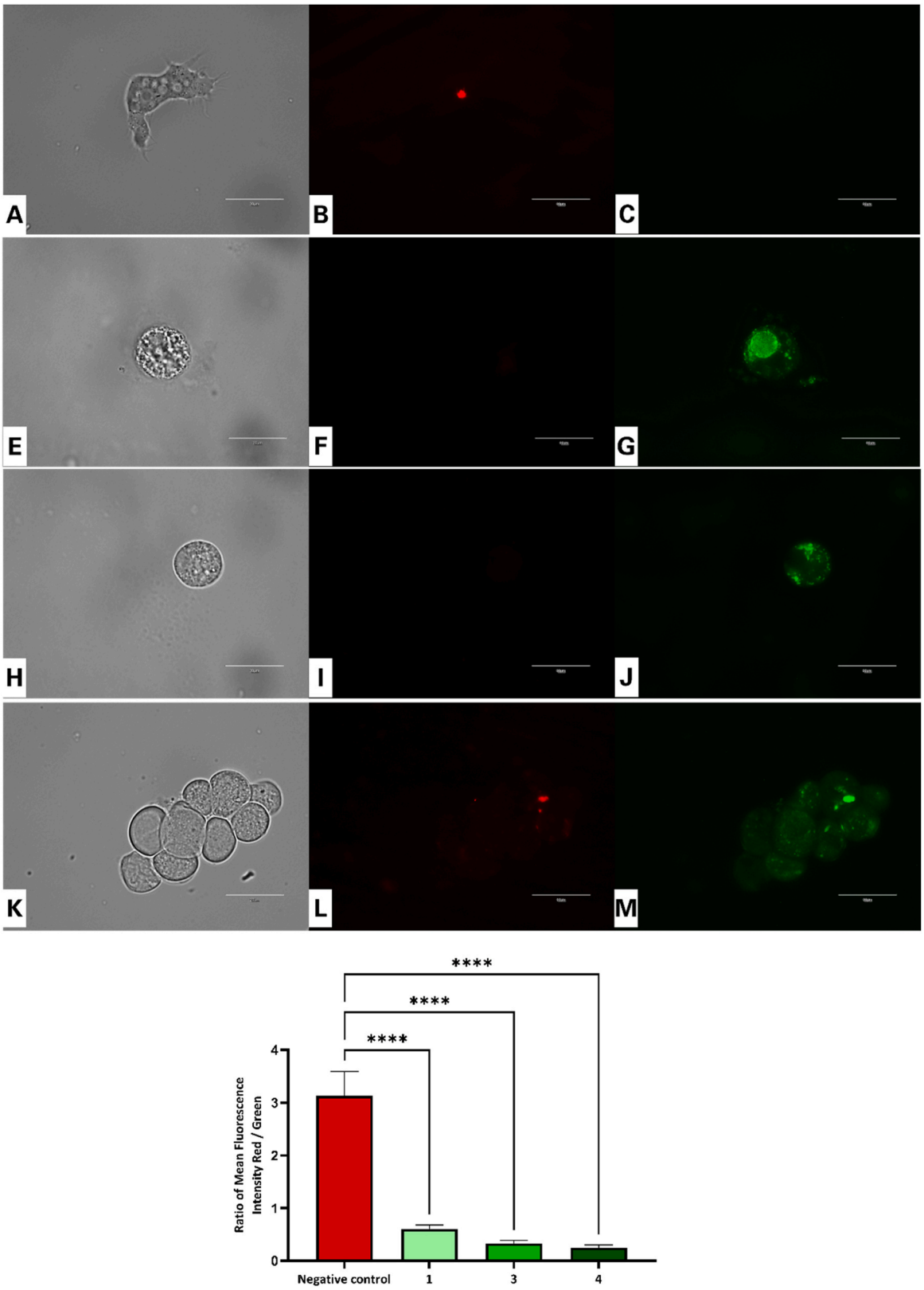

Fig. 8. Evaluation of the mitochondrial membrane potential using JC-1 dye in *Acanthamoeba polyphaga* trophozoites incubated with the IC_{90} of gongolarones A (1) (D, E, F), C (3) (G, H, I) and cystomexicone B (4) (J, K, L) for 24 h. Control cells (A, B, C). All images (100x) are based on EVOS™ FL Cell Imaging System M5000 (Scale Bar 20 μm). Data showed in the graph are presented as means ± SD, * ** * $p < 0.0001$; the results demonstrated significant differences when comparing treated cells to negative control. Differences between the values were assessed using One-Way Analysis of Variance (ANOVA). Mean fluorescence intensity of stained cells for each assay were determined using Fiji Software. All the experiments were conducted in triplicate.

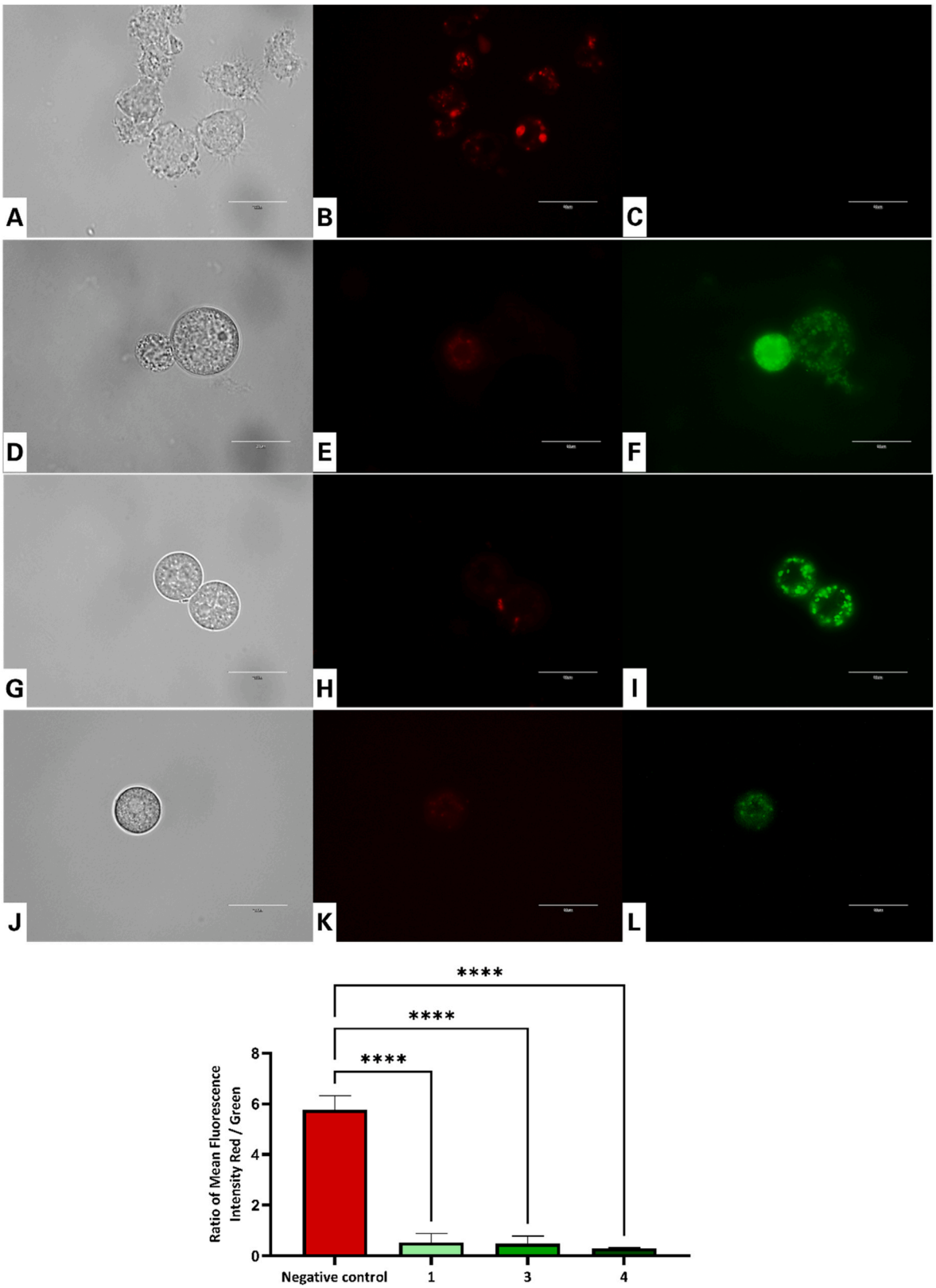

Fig. 9. Evaluation of the mitochondrial membrane potential using JC-1 dye in *Acanthamoeba griffini* trophozoites incubated with the IC_{90} of gongolarones A (1) (D, E, F), C (3) (G, H, I) and cystomexicone B (4) (J, K, L) for 24 h using. Control cells (A, B, C). All images (100x) are based on EVOS™ FL Cell Imaging System M5000 (Scale Bar 20 μm). Data showed in the graph are presented as means ± SD, * ** * $p < 0.0001$; the results demonstrated significant differences when comparing treated cells to negative control. Differences between the values were assessed using One-Way Analysis of Variance (ANOVA). Mean fluorescence intensity of stained cells for each assay were determined using Fiji Software. All the experiments were conducted in triplicate.

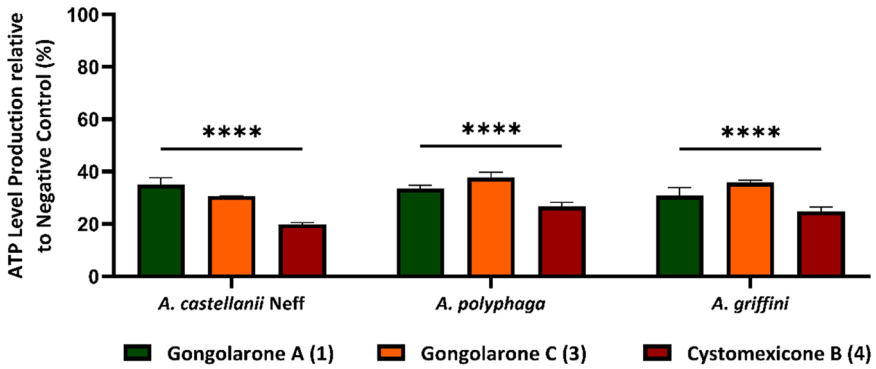

Fig. 10. ATP level production in *Acanthamoeba* spp. after the incubation with the IC_{90} of gongolarones A (1), C (3), and cystomexicone B (4) for 24 h using CellTiter-Glo® luminescent cell viability assay. All tested meroterpenes significantly decreased the level of mitochondrial ATP production in trophozoites of all tested *Acanthamoeba* compared with the negative control, $p < 0.0001$ (****).

aromatic moiety and two double bonds. Of note is the presence of three carbon signals at δ_C 82.5 (C-15), 79.7 (C-12) and 78.2 (C-14) due to oxygenated sp^3 carbons, which indicate the presence of an additional ring to complete the required degrees of unsaturation.

The analysis of the ^1H–^1H COSY (COrrelation SpectroscopY) and HMBC (Heteronuclear Multiple Bond Correlation) spectra and comparison with the diterpenoid 1′-methoxyamentadione (**5**) (Figs. S24-S25) [32] confirmed differences at the terminal end of the side chain of compound **1**. The COSY spectrum revealed the presence of one spin system from H_2-8 to H-14 (Fig. 2a). Key HMBC correlations from H_3-16 and H_3-17 with C-14 and C-15, from H-14 with C-12 and C-15, from H_2-13 with C-15, and those of H_3-18 with H-12 and H-10, confirmed the position of the oxygenated sp^3 carbon at δ_C 82.5 ppm (C-15) and its linkage through an ether bond with C-12 to form an oxolane (a tetrahydrofuran) ring (Fig. 2A).

The geometry of the double bonds and the relative configuration of the stereogenic centers C-12 and C-14 of compound **1** were determined by 1D-selective NOESY and 2D ROESY experiments. The *E* geometry of Δ^2 was supported by the ROE correlations observed between H_3-20 and methylene H_2-1, and that of H-2 with H_2-4. Additionally, the spatial correlation observed between H-6 and H_2-8 also confirmed the *E* geometry of Δ^6. The relative configuration of the five-membered ring was determined as 12*R** ,14*R** based on the NOE correlations of Me-18/H-12, H-12/H-13α and Me-17, and those of H-14/ H-13α and Me-17 (Fig. 2B).

Gongolarone B (**2**) was isolated as a colorless oil, optically active with $[\alpha]_D^{20}$ − 22 (*c* 0.17, $CHCl_3$). The HRESIMS showed a peak at *m/z* 479.2770 $[M+Na]^+$ (calc. $C_{28}H_{40}O_5Na$, 479.2773) which is in agreement with a molecular formula of $C_{28}H_{40}O_5$ and indicated nine degrees of unsaturation in the molecule. Its ^1H and ^{13}C NMR spectra (Table 1) revealed strong similarities with those of the linear diterpenoid 1′-methoxyamentadione (**5**) [32]. The most notable differences were found in fragment C-6-C-8, with signals for a methylene at H_2-6 ($\delta_{H\text{-}6}$ 3.13 (d, *J* = 5.0 Hz, 2 H); $\delta_{C\text{-}6}$ 46.3) and one olefinic proton H-8 ($\delta_{H\text{-}8}$ 5.30 (ddd, *J* = 7.2, 7.2, 0.9 Hz, 1 H); $\delta_{C\text{-}8}$ 129.0). Compared to **5**, Me-19 of gongolarone B (**2**) showed shifted signals both in the ^1H and ^{13}C NMR experiments ($\delta_{H\text{-}19}$ 1.71 (d, *J* = 0.9 Hz); δ_C 24.6), as well as the carbon chemical shift of the ketone at C-5 (δ_C 208.7 ppm). All these data indicated a double bond isomerization at C-7-C-8 which was confirmed in the COSY experiment with the observed spin system from H-8 to H-11 in the COSY experiment, and the HMBC correlations observed between H-6 with C-5, C-9 and C-19. The analysis of ^2D NMR experiments confirmed the full planar structure of **2** (Fig. 1).

Gongolarone C (**3**), $[\alpha]_D^{20}$ − 14 (*c* 0.04, $CHCl_3$), possessed the molecular formula $C_{28}H_{40}O_5$ and nine degrees of unsaturation, as deduced from the sodium adduct observed at the HRESIMS. Analysis of the ^1H and ^{13}C NMR data (Table 1) resemble those of its isomers gongolarone B (**2**) and 1′-methoxyamentadione (**5**) [32], which confirmed the characteristic signals of the toluhydroquinone moiety, and the same C-5-C-17 fragment of compound **5**. The most remarkable differences were found at positions C-1-C-4. The characteristic methylene H_2-1 is upfield shifted ($\delta_{H\text{-}1}$ 2.70 (ddd, *J* = 10.2, 5.9, 3.3 Hz); $\delta_{C\text{-}1}$ 28.4) and coupled with methylene H_2-2 ($\delta_{H\text{-}2a}$ 2.86 (m); $\delta_{H\text{-}2a}$ 2.77 (m); $\delta_{C\text{-}2}$ 35.2). Also, one olefinic proton is attributed to H-4 ($\delta_{H\text{-}4}$ 6.04 (d, *J* = 1.3 Hz); $\delta_{C\text{-}8}$ 126.5) which shows a long-range coupling with Me-20 ($\delta_{H\text{-}20}$ 1.86 (d, *J* = 1.3 Hz); δ_C 25.3). The HMBC correlations of Me-20 with C-2 and C-4, and those of H-4 with C-2 and C-5 established the presence of a double bond at C-3-C-4, and confirmed a singular conjugated 3*E*,6*E*-3,7-dimethyl-5-one fragment to complete the planar structure of gongolarone C (**3**) (Fig. 1) after analysis of ^2D NMR experiments.

3.2. Configuration of gongolarones A-C (1–3) and meroterpenoids 5–6

The absolute configuration of the isolated gongolarones A-C (**1**-**3**) and meroterpenoids **5** and **6** was determined based on analysis of their specific rotations, comparison with data reported in the literature and by computational methods.

Except for gongolarone A (**1**), linear meroterpenoids **2**, **3**, **5** and **6** share the same C-9-C-18 terminal end that possess one single sterocenter at C-11. From a biogenetic perspective, all metabolites proceed from the same precursor, therefore the chirality at C-11 must be conserved in all of them. This aspect is key to compare physical properties of chiral compounds as is the specific rotation, and it is supported by the fact that the specific rotation of **2**, **3**, **5** and **6** have negative sign in all cases (see experimental Section 2.3). Therefore, in order to determine their absolute configuration, we analysed the specific rotation of simplified molecular models that contains a single sterocenter such as (*S*)-chichimol ketone, that contains a chiral α − methyl group attached to an α,β-unsaturated ketone, which absolute configuration was determined by enantioselective synthesis [47]. Since the specific rotation of (*S*)-(+)-chichimol ketone is positive, we could deduce that the absolute configuration of the stereogenic center of meroterpenoids **2**, **3**, **5** and **6** is 11*R*. Consequently, based on biogenetic considerations, we assume the same absolute configuration at C-11 for gongolarone A (**1**). Another example that supports this assignment is represented by isolated metabolites from *Aspergillus* species [48] (Fig. 3).

Furthermore, to fully determine the relative configuration of gongolarone A (**1**), quantum mechanical prediction of NMR data was used. In fact, theoretical calculations are an increasingly fast and reliable toolbox to address complex problems in structure determination of natural products [49]. A comparison between experimental and calculated values for a set of putative candidates underpins these methods. Among the different tools available, those based on Bayesian analysis such as the seminal DP4 probability or the more recently proposed DP4 + and *J*-DP4 methods, stand out for their first-rate performance[33,34,50].

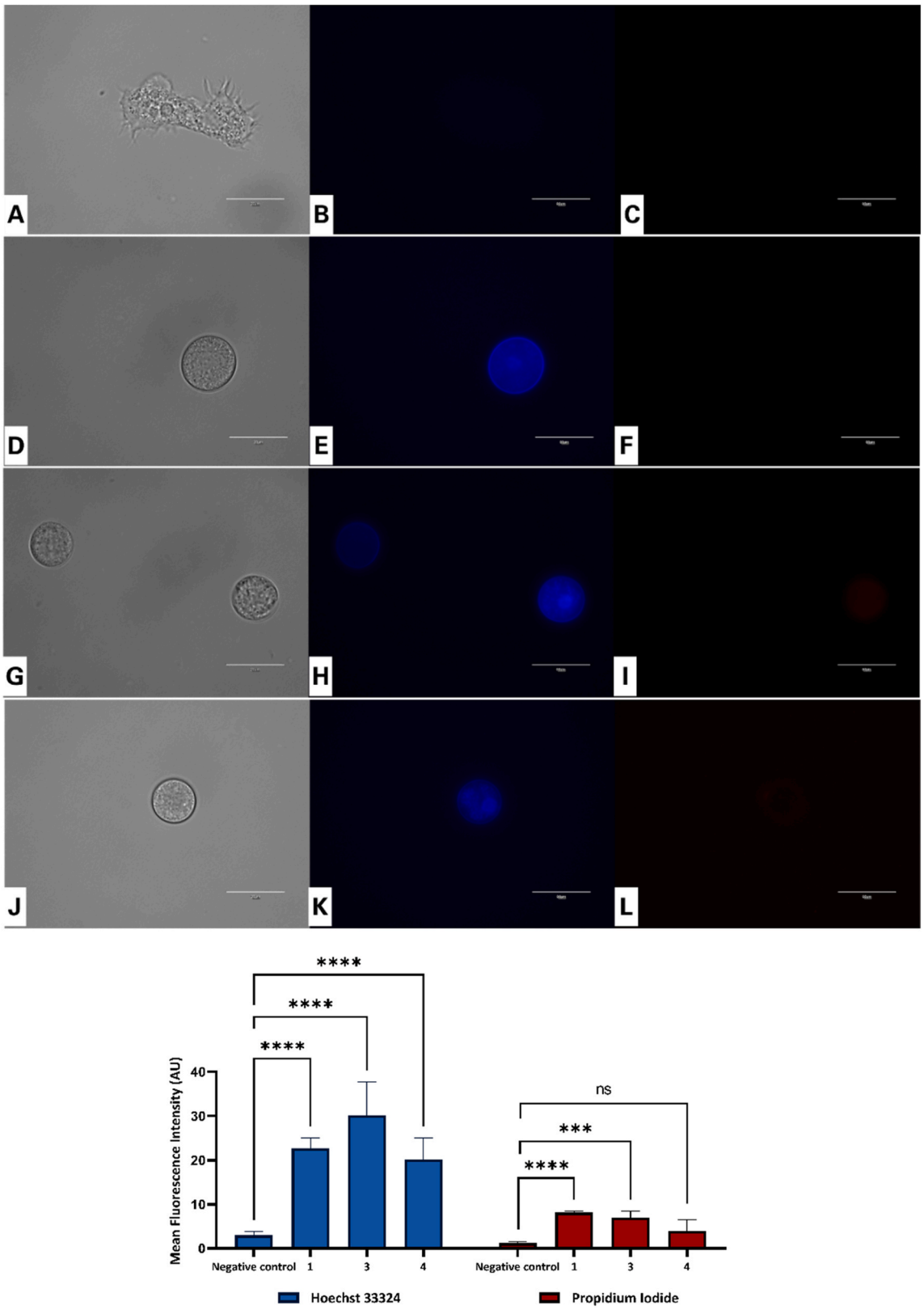

Fig. 11. Effect of IC_{90} of gongolarones A (1) (D, E, F), C (3) (G, H, I) and cystomexicone B (4) (J, K, L) in trophozoites of *Acanthamoeba castellanii* Neff using Hoechst 33342/PI apoptosis detection kit, incubated for 24 h. The nuclei of treated cells stained with a bright-blue fluorescence, evidencing cells undergoing PCD. IP showed in treated cells emitting a red fluorescence, suggest a late apoptosis. All images (100x) are based on EVOS™ FL Cell Imaging System M5000 (Scale Bar 20 μm). The graph represents the mean fluorescence intensity (AU) of cells stained by Hoechst 33324 / PI kit. Differences between the values were assessed using One-Way Analysis of Variance (ANOVA). Data are presented as means ± SD, ns: non-significant, * ** $p < 0.001$, * ** * $p < 0.0001$; the result showed significant differences when comparing treated cells stained with Hoechst dye to negative control. Mean fluorescence intensity of stained cells for each assay were determined using Fiji Software. All the experiments were conducted in triplicate.

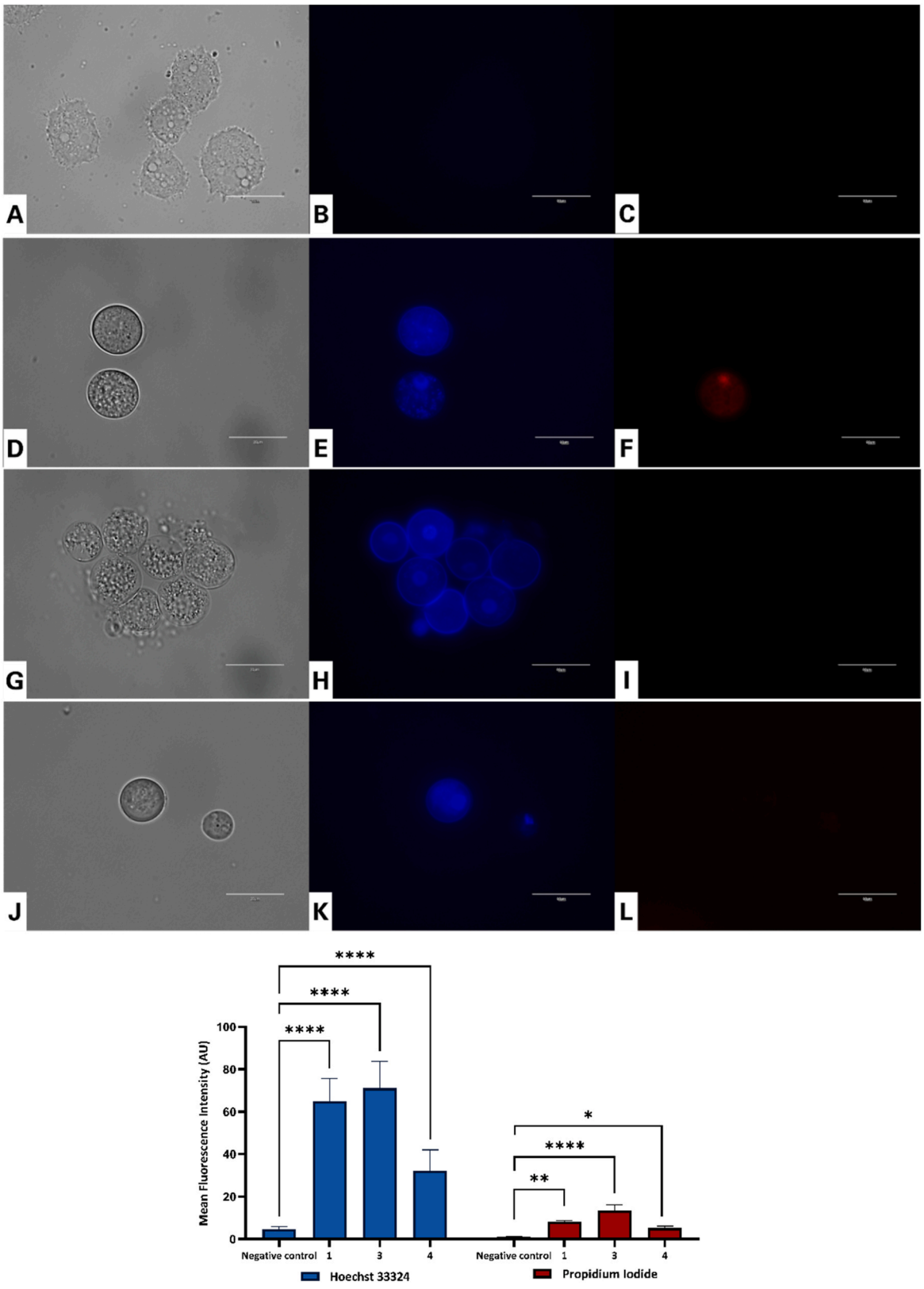

Fig. 12. Evaluation of chromatin condensation using Hoechst 33342/PI apoptosis detection kit in *Acanthamoeba polyphaga* trophozoites, incubated with the IC_{90} of gongolarones A (1) (D, E, F), C (3) (G, H, I) and cystomexicone B (4) (J, K, L) for 24 h. Control cells (A, B, C). All images (100x) are based on EVOS™ FL Cell Imaging System M5000 (Scale Bar 20 μm). Data showed in the graph are presented as means ± SD, * $p < 0.05$, * * $p < 0.01$, * ** * $p < 0.0001$; the results demonstrated significant differences when comparing treated cells to negative control. Differences between the values were assessed using One-Way Analysis of Variance (ANOVA). Mean fluorescence intensity of stained cells for each assay were determined using Fiji Software. All the experiments were conducted in triplicate.

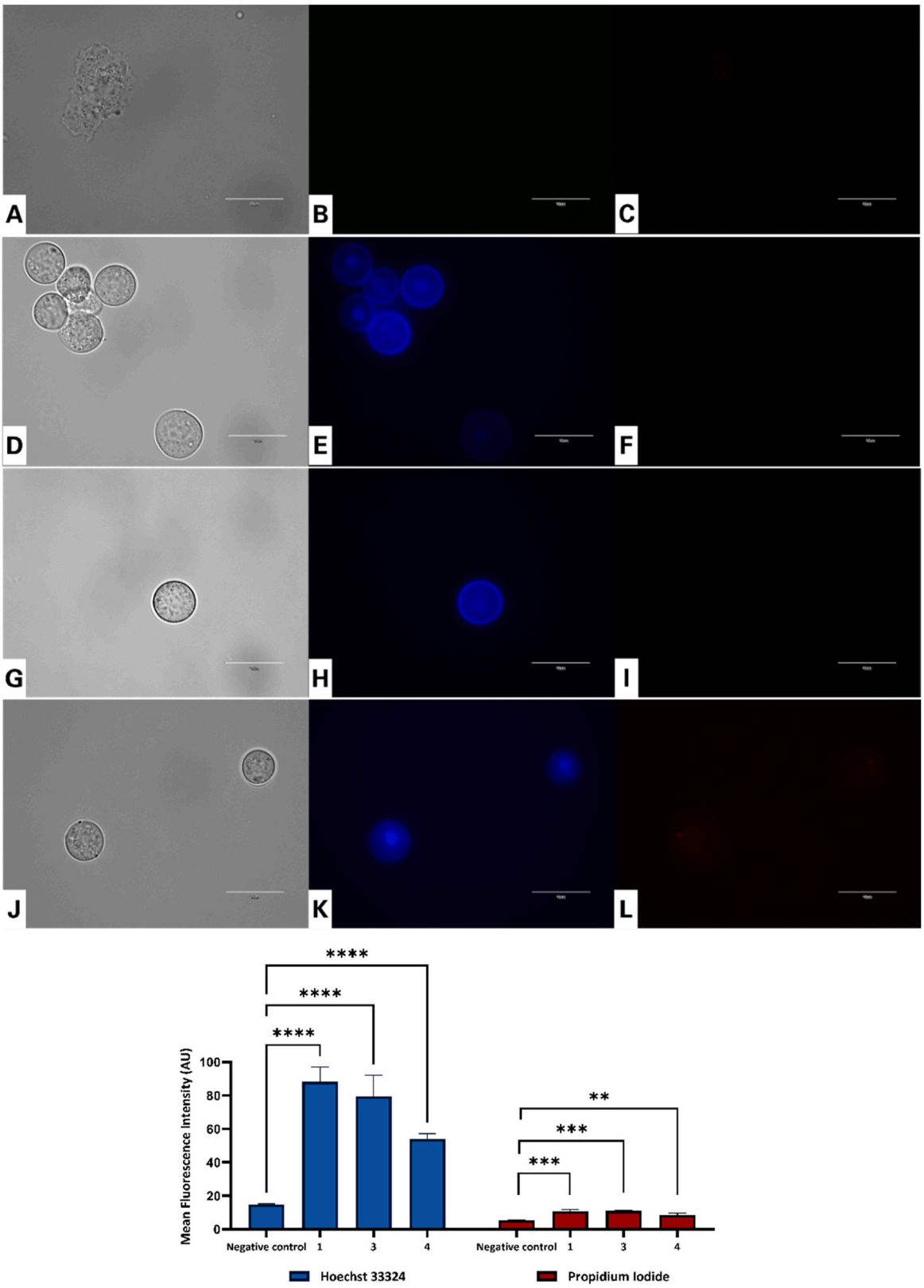

Fig. 13. Evaluation of chromatin condensation using Hoechst 33342/PI apoptosis detection kit in *Acanthamoeba griffini* trophozoites, incubated with the IC_{90} of gongolarones A (1) (D, E, F), C (3) (G, H, I) and cystomexicone B (4) (J, K, L) for 24 h. Control cells (A, B, C). All images (100x) are based on EVOS™ FL Cell Imaging System M5000 (Scale Bar 20 μm). Data showed in the graph are presented as means ± SD, * * $p < 0.01$, * ** $p < 0.001$, * ** * $p < 0.0001$; the results demonstrated significant differences when comparing treated cells to negative control. Differences between the values were assessed using One-Way Analysis of Variance (ANOVA). Mean fluorescence intensity of stained cells for each assay were determined using Fiji Software. All the experiments were conducted in triplicate.

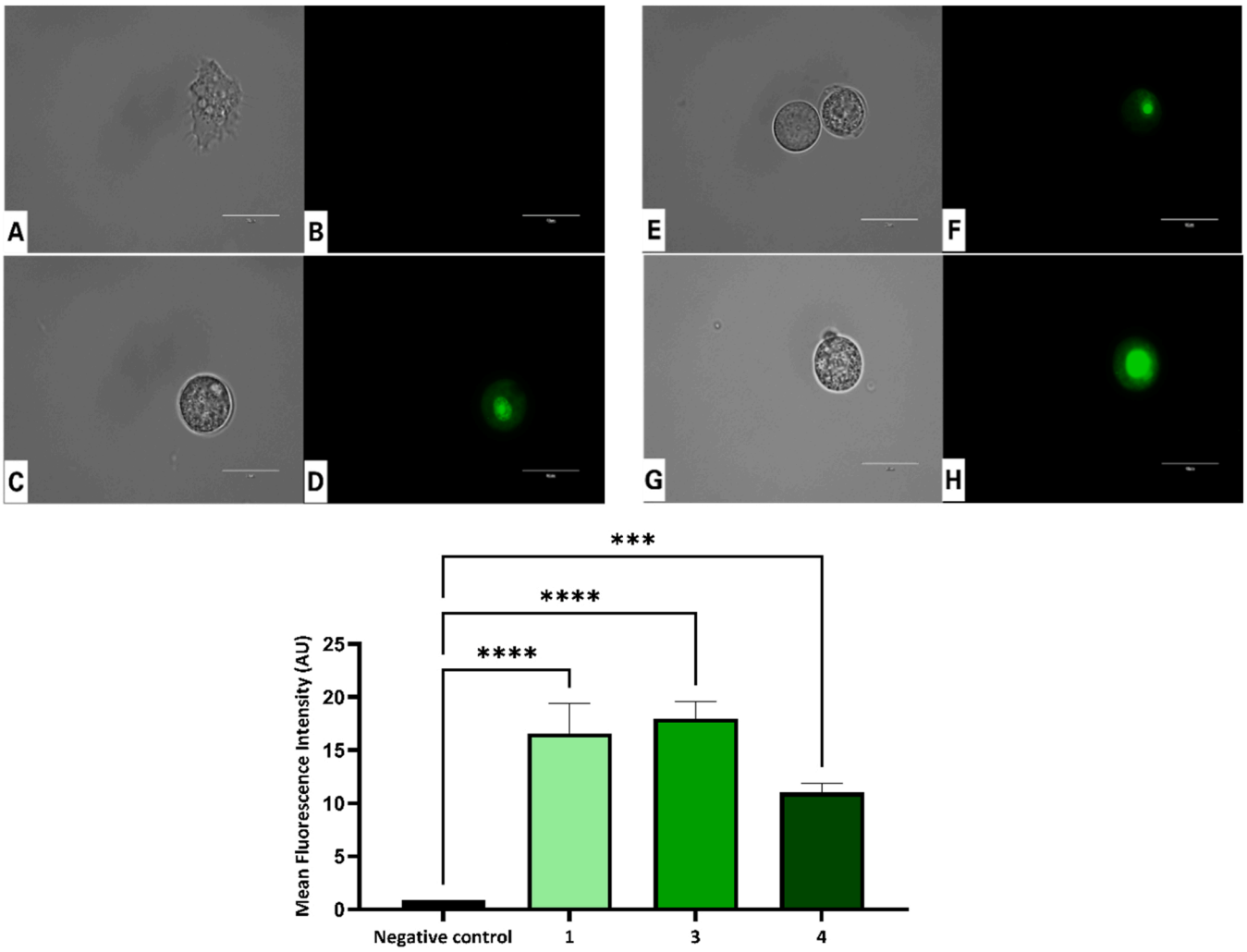

Fig. 14. Effect of IC_{90} of gongolarones A (1) (C, D), C (3) (E, F) and cystomexicone B (4) (G, H) on the membrane permeability of *Acanthamoeba castellanii* Neff compared with the control (A, B), using SYTOX™ Green assay after 24 h of incubation. Treated cells emitted green fluorescence, indicating alterations on the permeability of the plasmatic membrane. All images (100x) are based on EVOS™ FL Cell Imaging System M5000 (Scale Bar 20 μm). The graph includes the mean fluorescence intensity (AU) emitted by the cells stained using SYTOX™ Green reagent. Differences between the values were assessed using One-Way Analysis of Variance (ANOVA). Data are presented as means ± SD, * ** $p < 0.001$, * ** * $p < 0.0001$; the results showed significant differences when comparing treated cells to negative control. Mean fluorescence intensity of stained cells for each assay were determined using Fiji Software. All the experiments were conducted in triplicate.

Considering that all stereogenic centers in gongolarone A (**1**) were located relatively close to each other on one side of the molecule, we used a fragment-based approach to reduce the computational cost [51]. Thus, all possible diasteroisomers of the C-9-C-18 moiety (fragments F1-F4, SI section S2) were generated and thorough conformational sampling for each one was undertaken using a mixed torsional/low-mode algorithm and the Merck molecular force field. All conformations found within a 21 kJ/mol energy threshold were used to predict their NMR parameters ($^3J_{HH}$ and magnetic shielding constants to obtain chemical shifts) by DFT calculations at the B3LYP/G-31 G* level of theory as required in the *J*-DP4 methods. Furthermore, geometrical optimization followed by NMR calculations at the PCM/mPW1PW91/6–31 +G(d,p)//B3LYP/6–31 G* level of theory was also done as described in the DP4 + methods. Among all the stereoisomers tested, fragment 11*R** ,12*R** ,14*R** showed the best match with the experimental data. This configuration showed the smallest corrected mean absolute errors (CMAE) as well as the highest *J*-DP4 and DP4 + probabilities (> 99.9% overall probability) to represent the real structure (SI sections S3-S5). This result is in good agreement with the dipolar correlations observed in the ROESY experiment and allowed us to propose the absolute configuration of chiral centers of gongolarone A (**1**) as 11*R*, 12*R*, 14*R*.Fig. 4.

3.3. *In vitro evaluation of the amoebicidal effect and cytoxicity of tested meroterpenes 1-6*

The amoebicidal potential of meroterpenes gongolarones A (**1**), B (**2**), C (**3**), cystomexicone B (**4**), 1′-methoxyamentadione (**5**) and 6*Z*-1′-methoxyamentadione (**6**), were tested *in vitro* against the infective stages, trophozoites and cysts, of species *Acanthamoeba castellanii, A. polyphaga* and *A. griffini* (Table 2).

The results showed in Table 2 revelated that all tested compound demonstrated antiamoebic activity against the tree strains of *Acanthamoeba* spp. The gongolarones A (**1**) and C (**3**) showed the lowest Inhibitory Concentration 50 (IC_{50}) value against the trophozoite and cyst stage of all tested *Acanthamoeba* strains. The compound **1** was the most active compound against trophozoite and cyst stage of *A. castellanii* Neff (3.99 ± 0.14 and 10.44 ± 0.04 μM, respectively), and for the trophozoite stage of clinical strains *A. polyphaga* (5.43 ± 0.30 μM) and *A. griffini* (2.61 ± 0.16 μM). Beside this, **3** was the most active compound against the cyst stage of *A. polyphaga* and *A. griffini* (6.85 ± 0.52 and 10.05 ± 0.56 μM, respectively). Gongolarone B (**2**), 1′-

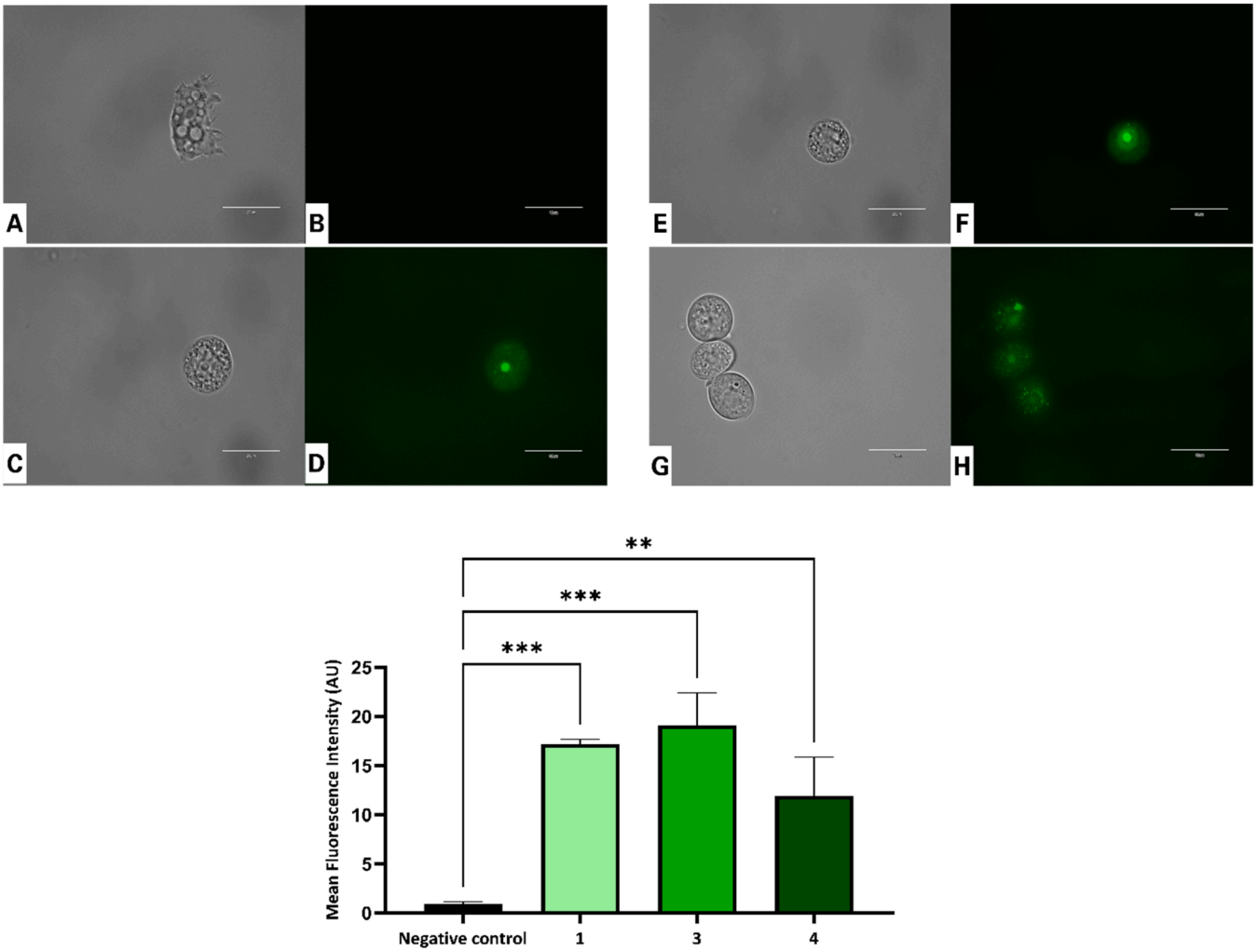

Fig. 15. Evaluation of membrane permeability using SYTOX™ Green assay in *Acanthamoeba polyphaga* trophozoites, incubated with the IC_{90} of gongolarones A (1) (C, D), C (3) (E, F) and cystomexicone B (4) (G, H) for 24 h. Control cells (A, B). All images (100x) are based on EVOS™ FL Cell Imaging System M5000 (Scale Bar 20 μm). Data showed in the graph are presented as means ± SD, * * $p < 0.01$, * ** $p < 0.001$; the results demonstrated significant differences when comparing treated cells to negative control. Differences between the values were assessed using One-Way Analysis of Variance (ANOVA). Mean fluorescence intensity of stained cells for each assay were determined using Fiji Software. All the experiments were conducted in triplicate.

methoxyamentadione (**5**), and 6*Z*-1′-methoxyamentadione (**6**) showed low amoebicidal activity compared to **1** and **3**. Cystomexicone B (**4**) only revelated amoebicidal effect on trophozoites and cyst stage of *A. castellanii* Neff, and on the trophozoites of *A. griffini* (51.44 ± 3.63 μM). Whereas compound **4** showed a low amoebic activity against trophozoite and cyst stage of clinical strain *A. polyphaga* and cyst of *A. griffini,* demonstrated IC_{50} values more than 100 μM.

On the other hand, all tested meroterpenes revelated no cytotoxic effect on murine macrophages cell line J774A.1. Gongolarones A (**1**), C (**3**), and cystomexicone B (**4**) demonstrated a Cytotoxic Concentration 50 (CC_{50}) value higher than 400 μM. Notwithstanding, compounds **2**, **5** and **6** exhibited similar CC_{50} values related to IC_{50} values in trophozoites (Table 2).

To evaluate the mechanism of action on the cell, and the induction of mechanism of Programmed Cell Dead (PCD) on *Acanthamoeba*, gongolarones A (**1**), C (**3**), and cystomexicone B (**4**) were selected. The trophozoites of *A. castellanii* Neff, *A. polyphaga* and *A. griffini* were incubated with the IC_{90} of tested meroterpenes (Table 3).

3.4. Evaluation of actin cytoskeleton distribution in treated Acanthamoeba trophozoites

The cell treated with gongolarones A (**1**) and C (**3**) showed an effect on the actin networks. Trophozoites fixed and staining with phalloidin-TRITC exhibited orange fluorescence. In treated cell incubated with the IC_{90} of compounds **1** and **3** for 24 h, suggesting that the actin cytoskeleton is much less organized (Fig. 5, central and right columns). Moreover, trophozoites emitted a lower orange fluorescence relative to the healthy cells, which showed a normal conformation of the actin networks (Fig. 5, left column).

3.5. Evaluation of the intracellular tubulin organization in the tested strains of Acanthamoeba

Tubulin antibodies using for staining the trophozoites revealed red fluorescence. Inside of cells incubated with the IC_{90} of gongolarones A (**1**) and C (**3**) for 24 h, suggesting a destruction or disorganization of the tubulin microtubules (Fig. 6, central and right columns). On the other hand, trophozoites in the negative control showed a normal organization of the tubulin microtubules (Fig. 6, left column). Moreover, the added drop of mounting DAPI solution stain the double stranded DNA

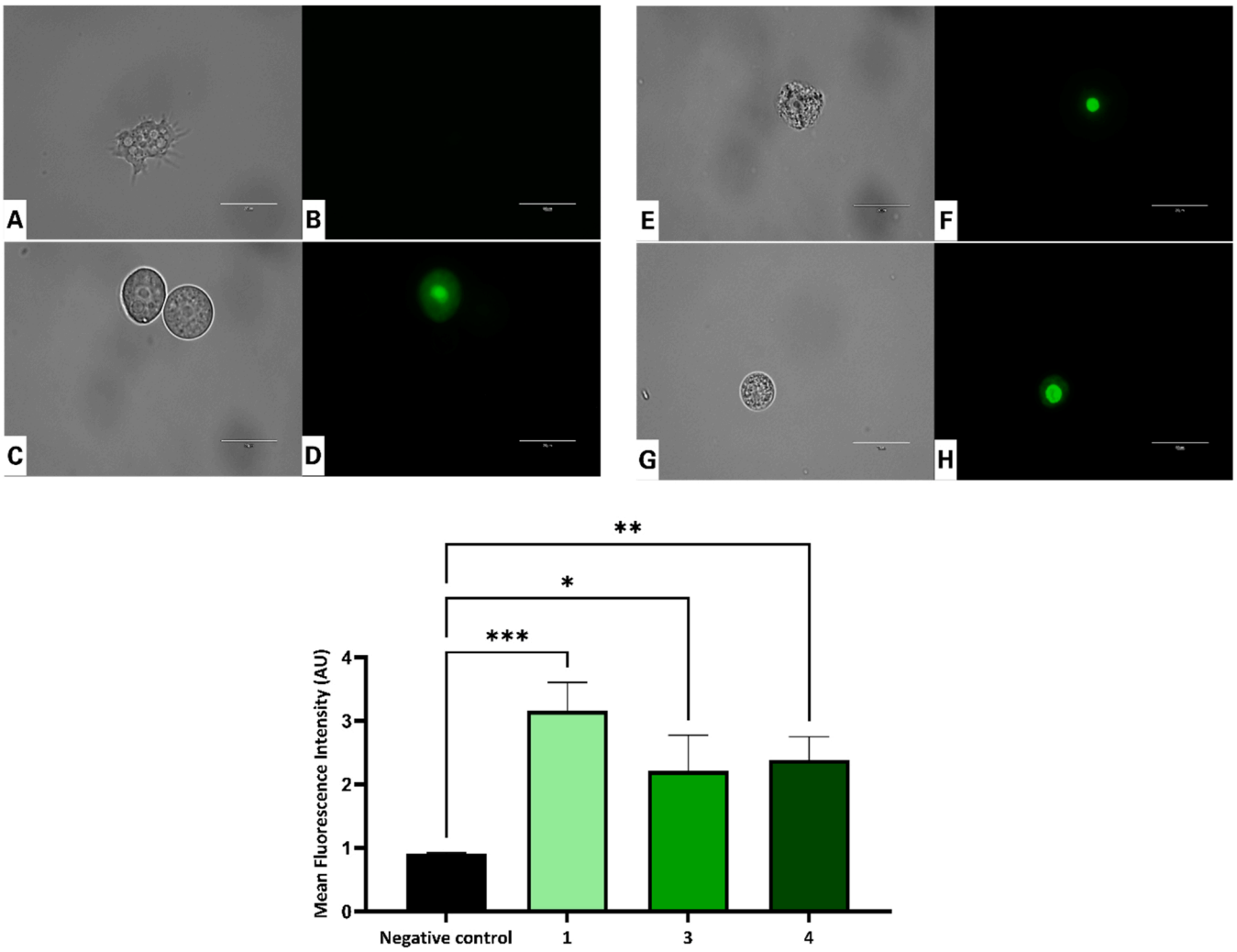

Fig. 16. Evaluation of membrane permeability using SYTOX™ Green assay in *Acanthamoeba griffini* trophozoites, incubated with the IC_{90} of gongolarones A (1) (C, D), C (3) (E, F) and cystomexicone B (4) (G, H) for 24 h. Control cells (A, B). All images (100x) are based on EVOS™ FL Cell Imaging System M5000 (Scale Bar 20 μm). Data showed in the graph are presented as means ± SD, * $p < 0.05$, ** $p < 0.01$, *** $p < 0.001$; the results demonstrated significant differences when comparing treated cells to negative control. Differences between the values were assessed using One-Way Analysis of Variance (ANOVA). Mean fluorescence intensity of stained cells for each assay were determined using Fiji Software. All the experiments were conducted in triplicate.

emitting a blue fluorescence in treated and healthy cells.

3.6. Gongolarones A (1), C (3), and cystomexicone B (4) caused mitochondrial malfunction in treated Acanthamoeba trophozoites

As illustrated in the Figs. 7–9 and S27-S29 (right column), the gongolarones A (**1**), C (**3**), and cystomexicone B (**4**) could depolarize the mitochondrial membrane potential by inhibition of JC-1 agglomeration in *Acanthamoeba castellanii* Neff, *A. polyphaga* and *A. griffini* trophozoites. JC-1 dye remained in the cytoplasm in its monomeric form with an emission of green fluorescence. Moreover, in untreated healthy cells of the negative control showed in the Figs. 7–9 and S27-S29 (A-C), the dye shown mitochondria aggregations with a red fluorescence. The mean fluorescence intensity value of red and green fluorescence emitted by the aggregate form and monomer form of JC-1 stained trophozoites were determined. Then, the ratio between the red and green fluorescence was calculated and represented for each JC-1 assay on *Acanthamoeba castellanii* Neff, *A. polyphaga* and *A. griffini.* In the tree tested strains of this study, the results obtained demonstrated significant differences between the mean red/green fluorescence intensity values produced by trophozoites treated with compounds **1**, **3** and **4**, and the mean values emitted by negative control cells; * ***$p < 0.0001$ (Figs. 7–9).

3.7. Measurement of ATP

Healthy cells need a suitable level of ATP for a correct functioning of the mitochondria. Production of ATP was measuring in control cells untreated and in cells incubated for 24 h with the IC_{90} of gongolarones A (**1**), C (**3**), and cystomexicone B (**4**) (Fig. 10). The results showed that this tree molecules induced a reduction of ATP production in all tested strains of *Acanthamoeba.* A One-Way analyses variance (ANOVA) was carried out to test the statistical differences between means. All compounds showed a highly significance decrease compared to the negative control, $p < 0.0001$ (****) (Fig. 10). Cystomexicone B (**4**) is the product that affected the most to *Acanthamoeba* spp. cells with values under of 20% for *A. castellanii* Neff and 25% for the clinical strain *A. griffini.*

3.8. Induction of chromatin condensation in the tested strains of Acanthamoeba

Obtained results are represented in the Figs. 11–13 and S30-S32. *Acanthamoeba* spp. trophozoites incubated with IC_{90} of the gongolarones A (**1**), C (**3**), and cystomexicone B (**4**) for 24 h showed a bright-blue staining nucleus (Figs. 11–13 and S30-S32, central columns). Chromatin condensation was evidenced in treated amoebae, whereas control cells

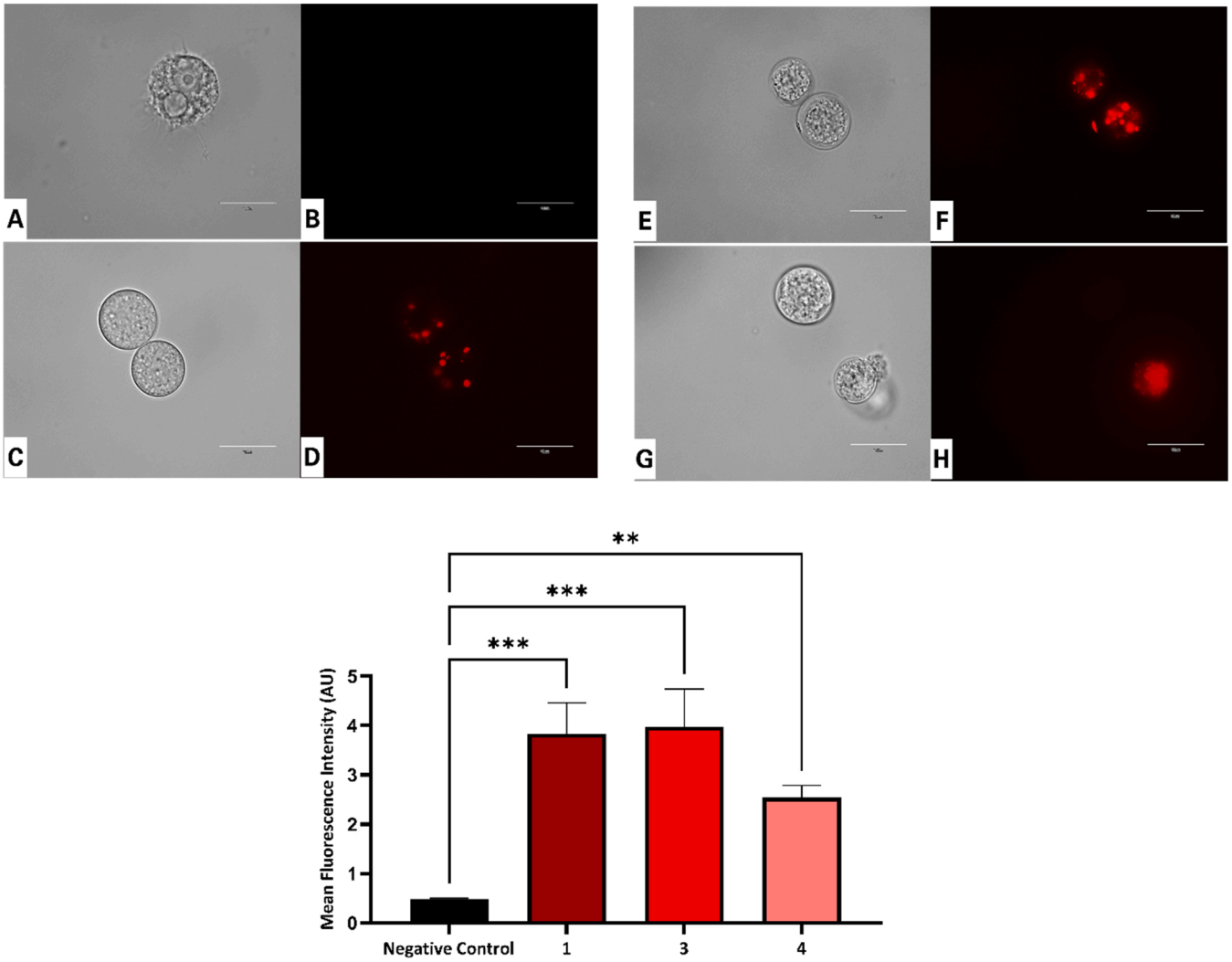

Fig. 17. Effect of IC_{90} of gongolarones A (1) (C, D), C (3) (E, F) and cystomexicone B (4) (G, H) on the production of Reactive Oxygen Species in *Acanthamoeba castellanii* Neff compared with the control (A, B), using CellROX® Deep Red fluorescent probe after 24 h of incubation. Treated cells showed an intense red fluorescence, indicating the production of ROS and suggesting the oxidatively stress of cells. All images (100x) are based on EVOS™ FL Cell Imaging System M5000 (Scale Bar 20 μm). The graph includes the mean fluorescence intensity (AU) emitted by the ROS produced by cells stained with CellROX® Deep Red reagent. Differences between the values were assessed using One-Way Analysis of Variance (ANOVA). Data are presented as means ± SD, * * $p < 0.01$, * ** $p < 0.001$; the results showed significant differences when comparing treated cells to negative control. Mean fluorescence intensity of stained cells for each assay were determined using Fiji Software. All the experiments were conducted in triplicate.

did not show any fluorescence (Figs. 11–13 and S30-S32, A-C). The propidium iodide (PI) showed a red fluorescence in treated cells, indicating a possible late apoptosis process (Figs. 11–13 and S30-S32, right columns). The mean values of blue and red fluorescence intensity were calculated for each assay using Hoechst 33324 and IP kit on treated cells and negative control. The data were represented in the graph of Figs. 11–13. The differences between the blue and red fluorescence produced by the treated cells with compounds **1**, **3** and **4**, and negative control were significant in all studied strains of *Acanthamoeba*; ****$p < 0.0001$, ***$p < 0.001$, ** $p < 0.01$ and * $p < 0.05$. Gongolarone C (**3**) was the molecule which demonstrated the highest mean values of blue and red fluorescence intensity in treated trophozoites of *A. castellanii* Neff and *A. polyphaga* for blue fluorescence, and *A. polyphaga* and *A. griffini* for red fluorescence. Additionally, cystomexicone B (**4**) showed the lowest mean values of fluorescence intensity in all tested strains of *Acanthamoeba,* revealing non-significant differences between the mean values of red fluorescence intensity emitted by treated trophozoites of *A. castellanii* Neff and negative control cells.

3.9. Evaluation of the plasma membrane damage in Acanthamoeba spp

SYTOX™ Green assay was used to detect damages induces by the incubation of amoebae with the IC_{90} of gongolarones A (**1**), C (**3**), and cystomexicone B (**4**) for 24 h (Figs. 14–16 and S33-S35). Treated cells showed green fluorescence on the tree *Acanthamoeba* strains after the treatment, indicating that the plasmatic membrane permeability has been altered (Figs. 14–16 and S33-S35, right columns). Nevertheless, the trophozoite integrity was maintained, avoiding the emptying of the cytoplasmatic content to the cytosol, evading the activation of host immune response. In the opposite, untreated cells showed total absence of fluorescence, which indicating a perfect membrane integrity (Figs. 14–16 and S33-S35; A, B). The graph represented in the Figs. 14–16 show the mean values of green fluorescence intensity produced by trophozoites of *Acanthamoeba* spp. Data indicated that the differences between the mean values of treated cells with compounds **1**, **3** and **4**, and negative controls cells were significant in all tested strains of *Acanthamoeba*; * $p < 0.05$, ** $p < 0.01$, *** $p < 0.001$ and **** $p < 0.0001$. Gongolarone C (**3**) demonstrated the highest mean

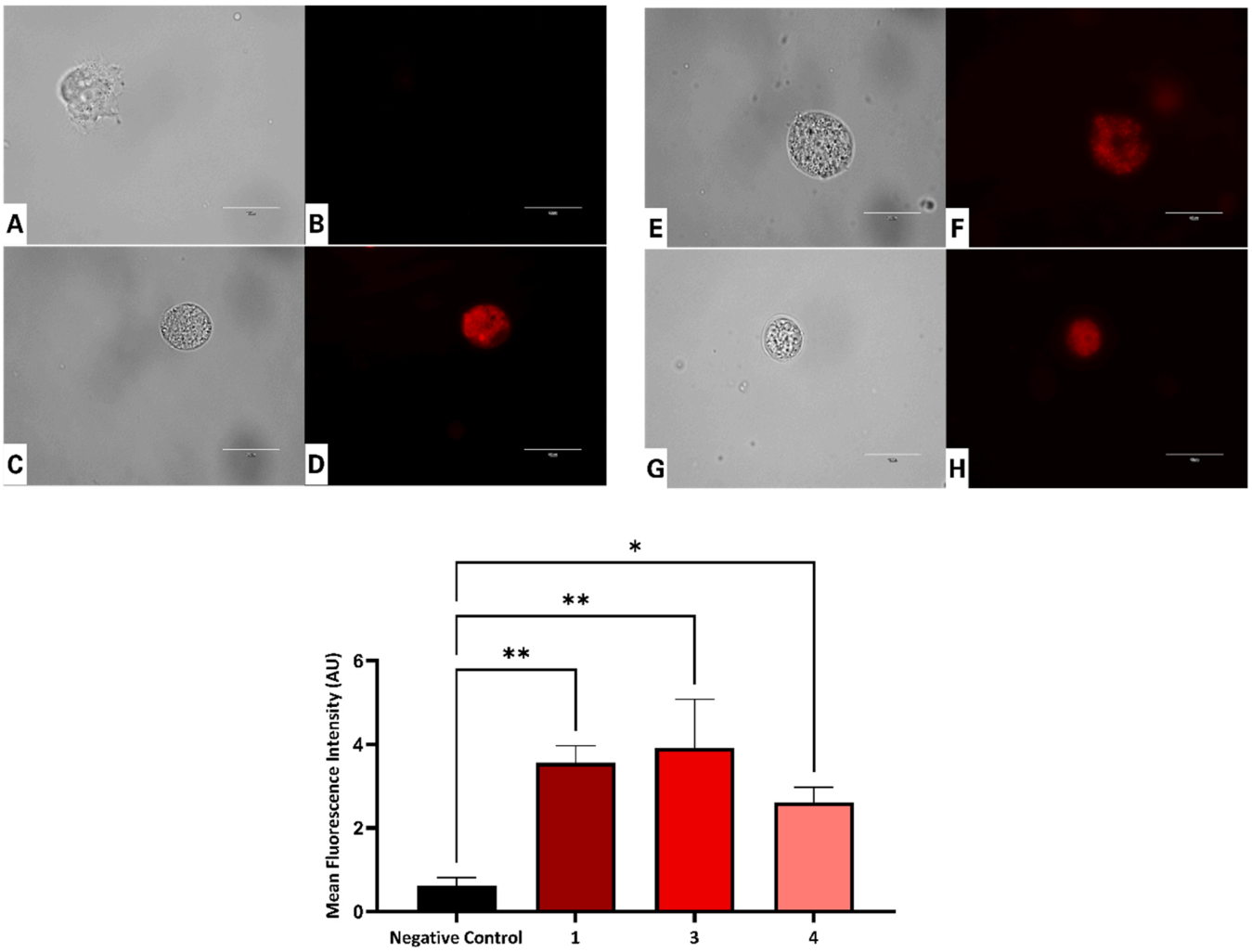

Fig. 18. Evaluation of membrane permeability using CellROX® Deep Red fluorescent probe in *Acanthamoeba polyphaga* trophozoites, incubated with the IC_{90} of gongolarones A (1) (C, D), C (3) (E, F) and cystomexicone B (4) (G, H) for 24 h. Control cells (A, B). All images (100x) are based on EVOS™ FL Cell Imaging System M5000 (Scale Bar 20 μm). Data showed in the graph are presented as means ± SD, * $p < 0.05$, ** $p < 0.01$; the results demonstrated significant differences when comparing treated cells to negative control. Differences between the values were assessed using One-Way Analysis of Variance (ANOVA). Mean fluorescence intensity of stained cells for each assay were determined using Fiji Software. All the experiments were conducted in triplicate.

values of green fluorescence intensity on trophozoites of *A. castellanii* Neff and *A. polyphaga.* Nonetheless, gongolarone A (**1**) emitted the highest green fluorescence intensity on *A. griffini* trophozoites (Figs. 14–16).

3.10. Gongolarones A (1), C (3), and cystomexicone B (4) induce the formation of ROS in Acanthamoeba

The obtained results represented in Figs. 17–19 and S36–38 demonstrated that the exposure to the IC_{90} of gongolarones A (**1**), C (**3**), and cystomexicone B (**4**) after 24 h, induced the production of Reactive Oxygen Species (ROS) in trophozoites of *Acanthamoeba* tested strains. Treated cells showed an intense red fluorescence (Figs. 17–19 and S36–38, right columns), whereas healthy cells presented absence of fluorescence (Figs. 17–19 and S35-S38; A, B). Mean values of deep red fluorescence intensity emitted by cells were determined and represented in the graph of Figs. 17–19**.** The results obtained showed significant differences between the mean values of all *Acanthamoeba* spp. trophozoites treated with compounds **1**, **3** and **4**, and the untreated cells; * $p < 0.05$, * * $p < 0.01$ and * ** $p < 0.001$. Trophozoites of *A. castellanii* Neff and *A. polyphaga* treated with compound **3** showed higher mean values of red fluorescence intensity than cells treated with molecules **1** and **4.** Additionally, trophozoites of *A. griffini* treated with gongolarone A (**1**) demonstrated more intense deep red fluorescence than those treated with **3** and **4.**

3.11. Effect of gongolarones A (1) and C (3) on the ultrastructure of Acanthamoeba

Trophozoites of *Acanthamoeba polyphaga* treated with gongolarones A (**1**) and C (**3**) presented alterations on morphology and on the normal ultrastructure of the cells. In images of Fig. 20 we observed mitochondrial and nuclear damage. Likewise, presence of multilamellar and multivesicular bodies, lipofuscin granules and vacuoles with cellular content, indicate that autophagy process occurred within treated trophozoites. Recently, autophagy process is considering as a multifaceted regulator of different cell death mechanisms [52–54]. Wu *et al.* (2018) demonstrated that some oleic acids tiggered apoptosis in *A. castellanii* by the induction of autophagy process and activation of uncoupling proteins [55]. In this sense, the results obtained in this study suggesting that compounds **1** and **3** induce a PCD in trophozoites of *Acanthamoeba* spp. Therefore, autophagy process could be related to the regulation of PCD in trophozoites treated with gongolarones A (**1**) and C (**3**).Fig. 21.

On the other hand, images E, F, K and L of Fig. 20 represented the

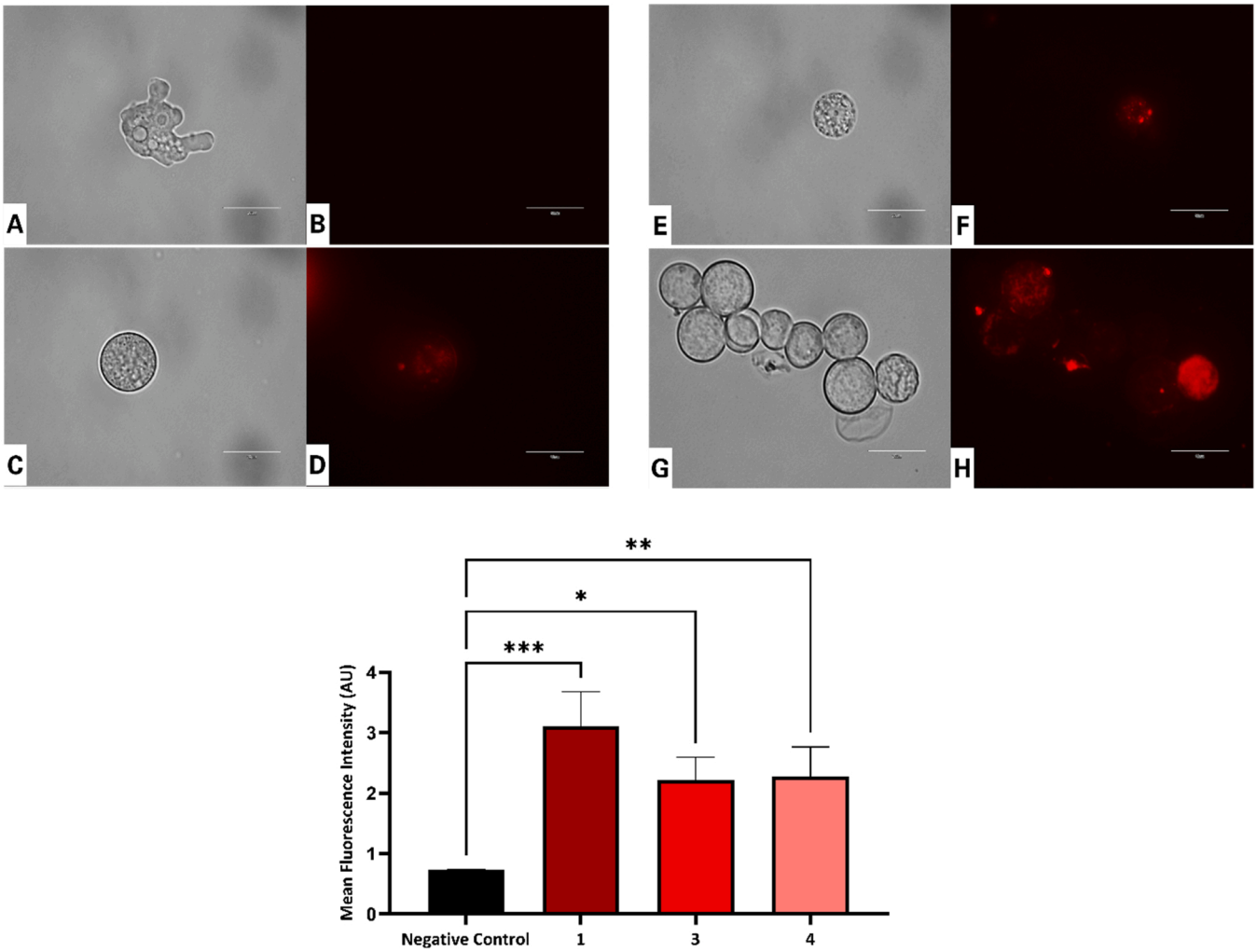

Fig. 19. Evaluation of membrane permeability using CellROX® Deep Red fluorescent probe in *Acanthamoeba griffini* trophozoites, incubated with the IC_{90} of gongolarones A (1) (C, D), C (3) (E, F) and cystomexicone B (4) (G, H) for 24 h. Control cells (A, B). All images (100x) are based on EVOS™ FL Cell Imaging System M5000 (Scale Bar 20 μm). Data showed in the graph are presented as means ± SD, * $p < 0.05$, * * $p < 0.01$, * ** $p < 0.001$; the results demonstrated significant differences when comparing treated cells to negative control. Differences between the values were assessed using One-Way Analysis of Variance (ANOVA). Mean fluorescence intensity of stained cells for each assay were determined using Fiji Software. All the experiments were conducted in triplicate.

formation of *Acanthamoeba polyphaga* precysts without the fully two characteristic cyst walls [56]. The presence of damaged precysts with autophagic vacuoles and glycogen granules were observed. Finally, the results obtained suggesting that trophozoites treated with gongolarones A (**1**) and C (**3**) inhibits the mature cyst walls developing of *Acanthamoeba polyphaga* during the encystment process.

3.12. Structure-activity relationship analysis

Meroterpenoids isolated from brown algae of *Gongolaria* (*Cystoseira*) genus have been scarcely tested against amoeba. In this work, six meroterpenoids have been isolated, among them, the new compounds gongolarones A-C (**1**-**3**) which antiamoeboid properties have been tested against different *Acanthamoeba* species. From the structural perspective, this family of compounds showed double bond isomerizations from $\Delta^{2\,t}$ to $\Delta^{3\,t}$ (green), from $\Delta^{6\,t}$ to Δ^{6c} and from $\Delta^{6\,t}$ to $\Delta^{7\,t}$ (purple). Comparison of gongolarone C (**3**) and 1′-methoxyamentadione (**5**) reveals that the isomerization $\Delta^{2\,t}$ to $\Delta^{3\,t}$ increases the antiamoeboid activity as well as the flexibility of the chain due to the presence of contiguous methylene fragments (red arrows). On the other hand, double bond isomerizations at C-6 do not contribute to an improvement in the anti-*Acanthamoeba* activity. Another structural feature found in this set of compounds are modifications in the terpenic chain. Loss of fragment C-12-C-16, cystomexicone B (**4**), diminished the antiparasitic effect, whereas cyclization by ether formation from C-12 to C-15 afforded the most active compound, gongolarone A (**1**).

4. Conclusions

Three new meroterpenes isolated from the brown algae *Gongolaria abies-marina* and identified as gongolarones A-C (**1**-**3**), together with the known cystomexicone B (**4**), 6*Z*-1′-methoxyamentadione (**5**) and 1′-methoxyamentadione (**6**), demonstrated amoebicidal activity against of *Acanthamoeba castellanii* Neff, *A. polyphaga* and *A. griffini.* We revealed that cyclization by ether formation from C-12 to C-15 of gongolarone A afforded the most active compound. Nevertheless, the isomerization $\Delta^{2\,t}$ to $\Delta^{3\,t}$ and presence of contiguous methylene fragments increases the antiamoeboid activity of gongolarone C (**3**). Gongolarones A (**1**), C (**3**) and cystomexicone B (**4**) induced PCD in trophozoites of *Acanthamoeba* tested in this study, showing chromatin condensation, mitochondrial damage, and oxidative stress remarkable by the cell ROS production. Novel compounds **1** and **3** disorganized the actin and tubulin networks of treated trophozoites. Additionally, those two molecules demonstrated that could inhibit the encystation of *Acanthamoeba.* Taking all the results

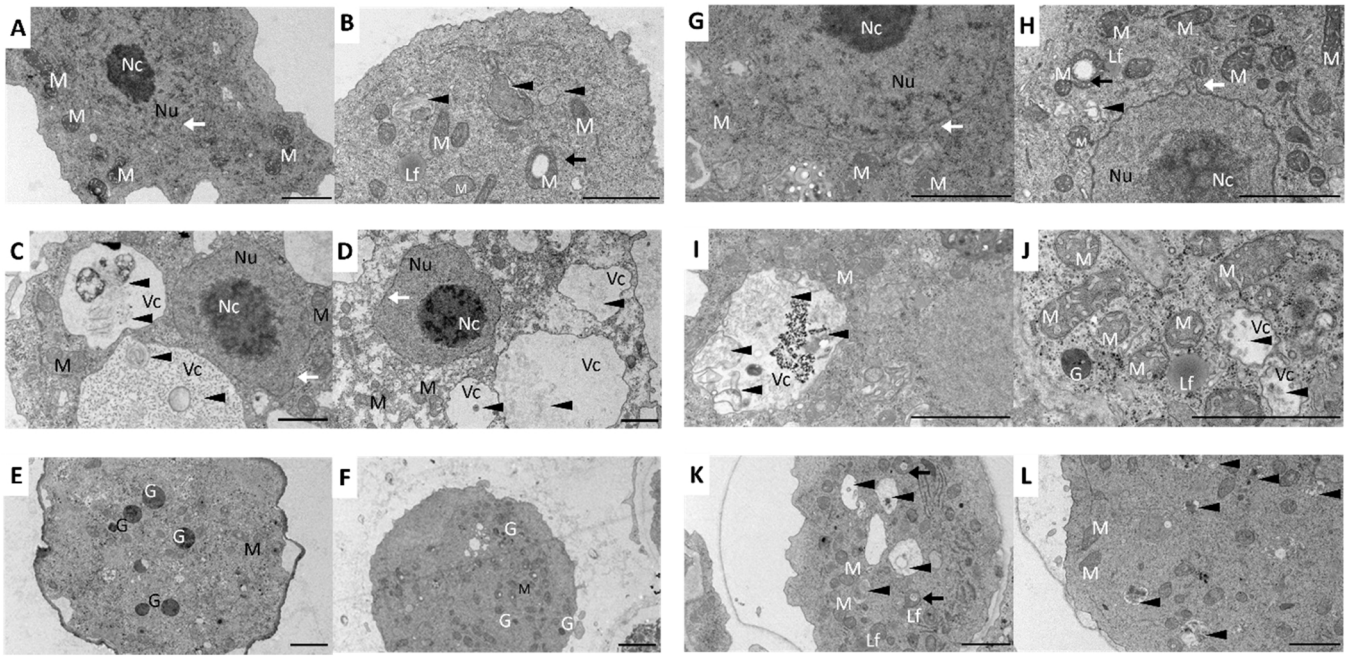

Fig. 20. Transmission electron microscopy (TEM) images of *Acanthamoeba polyphaga* trophozoites incubated with IC_{90} of gongolarones A (1) (B-F) and C (3) (H-L) for 24 h. Normal ultrastructure of whole cell in untreated trophozoites of A and G were observed. Nucleus (Nu) and nucleolus (Nc) presented normal conformation; nuclear membrane (white arrow) showed the characteristic morphology described in a healthy trophozoite. Mitochondria (M) presented normal shape of mitochondria cristae and matrix (A and G). In trophozoites treated with compounds 1 and 3 the presence of autophagic vacuoles (Vc), multivesicular and multilamellar bodies (black arrowhead), and lipofuscin granules (Lf) were observed, suggest that the trophozoites started autophagic process. Nuclear membrane of treated trophozoites (C, D and H; white arrows) showed altered conformation. Mitochondrial damage (M) was frequently observed. Trophozoites presented vacuolated mitochondria (black arrows), and mitochondrial swelling maintaining the integrity of the outer mitochondrial membrane. The presence of glycogen granules (G) was noted, normally observed during cyst formation process of *Acanthamoeba.* Images E, F, K and L showed damaged precyst after the treatment with compounds 1 and 3, did not fully presented the 2-distinct cyst walls. Images were obtained using a JEOL JEM-1011 transmission electron microscope (Scale Bar 2 μm).

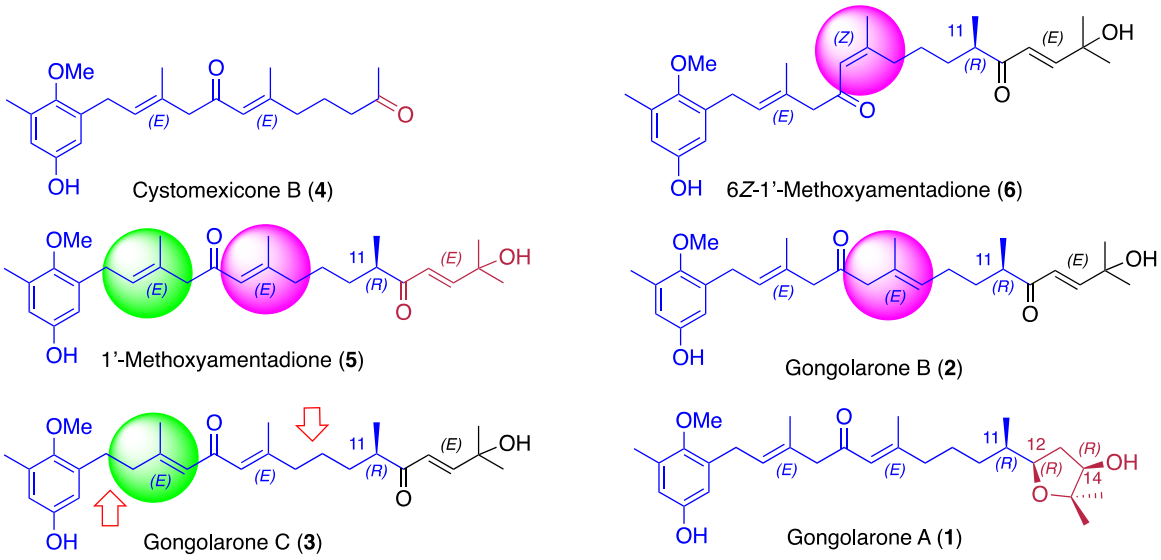

Fig. 21. Structure–activity relationship of meroterpenoids from *Gongolaria abies-marina* against *Acanthamoeba* species.

into account, seaweeds including *Gongolaria abies-marina* could be a source of bioactive marine molecules for developing new antiamoebic compounds against *Acanthamoeba.*

Funding

This study was supported funded by projects PID2019-109476RB-C21 (BIOALGRI) (Spanish Ministry of Science), Madrid, Spain; Fundación CajaCanarias–Fundación Bancaria "La Caixa" (2019SP52). Red de Investigación Cooperativa en Enfermedades Tropicales (RICET), Spain (project no. RD16/0027/0001 of the programe of Redes Temáticas de Investigación Cooperativa, FIS). Consorcio Centro de Investigación Biomédica en Red (CIBER), Área de Enfermedades Infecciosas (CIBERINFEC), Instituto de Salud Carlos III, 28029, Madrid, Spain (CB21/13/00100). Project No. 21/0587 funded by the Cabildo de Tenerife, Tenerife innova, Marco Estratégico de Desarrollo Insular

(MEDI) and Fondo de Desarrollo de Canarias (FDCAN). Project number ProID2021010118 funded by Agencia Canaria de Investigación, Innovación y Sociedad de la Información (ACIISI). RLRE was funded by a grant from ACIISI cofunded by Fondo Social Europeo (FSE) and FEDER, (TESIS2020010117). MOM was supported by the Programa de Apoyos para la Superación del Personal Académico de la UNAM (PASPA 2021) for carrying out the research stay between the Universidad de La Laguna and la Facultad de Estudios Superiores Iztacala.

CRediT author statement

Methodology, R.L.R.E; D.S.H. I.S; C.C.; L.S.V. and M.R.B; Software, R.L.R.E; I.S; C.C.; L.S.V. and M.R.B.; Validation, J.E.P.; M.O.M.; A.H.D.; A.R.D.M.; J.J.F. and J.L.M.; Formal analysis, J.E.P.; A.R.D.M.; J.J.F and J.L.M.; Investigation, R.L.R.E; D.S.H.; I.S and M.R.B; Resources, JEP and JLM.; Data curation, R.L.R.E; D.S.H.; C.C.; I.S and M.R.B; Writing – original draft preparation, R.L.R.E; D.S.H.; C.C.; I.S and M.R.B; Writing – review & editing, J.E.P.; M.O.M.; A.H.D.; A.R.D.M.; J.J.F. and JLM; Visualization, J.E.P. and J.L.M.; Supervision, J.E.P. and J.L.M.; Project administration, J.E.P. and J.L.M.; Funding acquisition, J.E.P.; A.R.D.M.; J.J.F and J.L.M. All authors have read and agreed to the published version of the manuscript.

Acknowledgements

Authors acknowledge Dr. M. Sansón for taxonomic identification of *Gongolaria abies-marina*. Dr. Adolfo Martínez-Palomo for the support provided to carry out the electron microscopy, as well as Dr. Martha Espinosa Cantellano for the facilities provided to establish and strengthen collaboration with CINVESTAV-Mexico and ULL. In addition, authors acknowledge the use of the facilities of the Galician Supercomputing Center (CESGA) provided by the CSIC. Cristina Cuadrado thanks ACIISI and FSE (Programa Operativo Integrado de Canarias 2014–2020, Eje 3, Tema Prioritario 74 – 85%) for a predoctoral fellowship.

Conflict of interest

The authors declare that there is not conflict of interest with the submission.

Appendix A. Supporting information

Supplementary data associated with this article can be found in the online version at doi:10.1016/j.biopha.2022.114185.

References

[1] W.H. Organization, Neglected tropical diseases, hidden successes, emerging opportunities, (2009). https://apps.who.int/iris/handle/10665/44214.
[2] D.B. McArthur, Emerging infectious diseases, Nurs. Clin. North Am. 54 (2019) 297–311, https://doi.org/10.1016/j.cnur.2019.02.006.
[3] N.I. Nii-Trebi, Emerging and neglected infectious diseases: insights, advances, and challenges, Biomed. Res. Int. 2017 (2017) 1–15, https://doi.org/10.1155/2017/5245021.
[4] G.S. Visvesvara, H. Moura, F.L. Schuster, Pathogenic and opportunistic free-living amoebae: Acanthamoeba spp., Balamuthia mandrillaris, Naegleria fowleri, and Sappinia diploidea, FEMS Immunol. Med. Microbiol. 50 (2007) 1–26, https://doi.org/10.1111/j.1574-695X.2007.00232.x.
[5] A. Samba-Louaka, V. Delafont, M.-H. Rodier, E. Cateau, Y. Héchard, Free-living amoebae and squatters in the wild: ecological and molecular features, FEMS Microbiol Rev. 43 (2019) 415–434, https://doi.org/10.1093/femsre/fuz011.
[6] R.A. Baquero, M. Reyes-Batlle, G.G. Nicola, C.M. Martín-Navarro, A. López-Arencibia, J. Guillermo Esteban, B. Valladares, E. Martínez-Carretero, J.E. Piñero, J. Lorenzo-Morales, Presence of potentially pathogenic free-living amoebae strains from well water samples in Guinea-Bissau, Pathog. Glob. Health 108 (2014) 206–211, https://doi.org/10.1179/2047773214Y.0000000143.
[7] R. Siddiqui, N.A. Khan, Biology and pathogenesis of Acanthamoeba, Parasit. Vectors 5 (2012) 6, https://doi.org/10.1186/1756-3305-5-6.
[8] A.G. de Lacerda, M. Lira, Acanthamoeba keratitis: a review of biology, pathophysiology and epidemiology, Ophthalmic Physiol. Opt. 41 (2021) 116–135, https://doi.org/10.1111/opo.12752.
[9] J. Lorenzo-Morales, N.A. Khan, J. Walochnik, An update on Acanthamoeba keratitis: diagnosis, pathogenesis and treatment, Parasite 22 (2015), https://doi.org/10.1051/parasite/2015010.
[10] A. Anwar, N.A. Khan, R. Siddiqui, Combating Acanthamoeba spp. cysts: what are the options? Parasit. Vectors 11 (2018) 26, https://doi.org/10.1186/s13071-017-2572-z.
[11] U. Ahmed, A. Anwar, S. Ong, A. Anwar, N.A. Khan, Applications of medicinal chemistry for drug discovery against Acanthamoeba infections, Med. Res. Rev. 42 (2022) 462–512, https://doi.org/10.1002/med.21851.
[12] S. Chen, R. Cai, Z. Liu, H. Cui, Z. She, Secondary metabolites from mangrove-associated fungi: source, chemistry and bioactivities, Nat. Prod. Rep. 39 (2022) 560–595, https://doi.org/10.1039/D1NP00041A.
[13] H.S. El-Beltagi, A.A. Mohamed, H.I. Mohamed, K.M.A. Ramadan, A.A. Barqawi, A. T. Mansour, Phytochemical and potential properties of seaweeds and their recent applications: a review, Mar. Drugs 20 (2022) 342, https://doi.org/10.3390/md20060342.
[14] A.C.S. Veríssimo, M. Pacheco, A.M.S. Silva, D.C.G.A. Pinto, Secondary metabolites from marine sources with potential use as leads for anticancer applications, Molecules 26 (2021) 4292, https://doi.org/10.3390/molecules26144292.
[15] J. Lorenzo-Morales, A.R. Díaz-Marrero, F. Cen-Pacheco, I. Sifaoui, M. Reyes-Batlle, M.L. Souto, A. Hernández Daranas, J.E. Piñero, J.J. Fernández, Evaluation of Oxasqualenoids from the Red Alga Laurencia viridis against Acanthamoeba, Mar. Drugs 17 (2019), https://doi.org/10.3390/md17070420.
[16] O. Chiboub, I. Sifaoui, M. Abderrabba, M. Mejri, J.J. Fernández, A.R. Díaz-Marrero, J. Lorenzo-Morales, J.E. Piñero, Apoptosis-like cell death upon kinetoplastid induction by compounds isolated from the brown algae Dictyota spiralis, Parasit. Vectors 14 (2021) 198, https://doi.org/10.1186/s13071-021-04693-7.
[17] H.S. Kalasariya, V.K. Yadav, K.K. Yadav, V. Tirth, A. Algahtani, S. Islam, N. Gupta, B.-H. Jeon, Seaweed-based molecules and their potential biological activities: an eco-sustainable cosmetics, Molecules 26 (2021) 5313, https://doi.org/10.3390/molecules26175313.
[18] S. Orellana, M. Hernández, M. Sansón, Diversity of Cystoseira sensu lato (Fucales, Phaeophyceae) in the eastern Atlantic and Mediterranean based on morphological and DNA evidence, including Carpodesmia gen. emend. and Treptacantha gen. emend, Eur. J. Phycol. 54 (2019) 447–465, https://doi.org/10.1080/09670262.2019.1590862.
[19] E.A. MOLINARI-NOVOA, M.D. GUIRY, Reinstatement of the genera Gongolaria Boehmer and Ericaria Stackhouse (Sargassaceae, Phaeophyceae), Not. Algarum 172 (2020) 1–10.
[20] V.L.M. Gouveia, A.M.L. Seca, M.C. Barreto, A.I. Neto, A. Kijjoa, A.M.S. Silva, Cytotoxic meroterpenoids from the macroalga Cystoseira abies-marina, Phytochem Lett. 6 (2013) 593–597, https://doi.org/10.1016/j.phytol.2013.07.012.
[21] J. Valdazo, M.A. Viera-Rodríguez, F. Tuya, Seasonality in the canopy structure of the endangered brown macroalga Cystoseira abies-marina at Gran Canaria Island (Canary Islands, eastern Atlantic), Eur. J. Phycol. 55 (2020) 253–265, https://doi.org/10.1080/09670262.2019.1696989.
[22] M.C. Barreto, E. Mendonça, V. Gouveia, C. Anjos, J.S. Medeiros, A.M.L. Seca, A. I. Neto, Macroalgae from S. Miguel Island as a potential source of antiproliferative and antioxidant products, Arquipelago Life Mar. Sci. 29 (2012) 53–58.
[23] V.L.M. Gouveia, A.M.L. Seca, M.C. Barreto, A.I. Neto, A. Kijjoa, A.M.S. Silva, Cytotoxic meroterpenoids from the macroalga Cystoseira abies-marina, Phytochem Lett. 6 (2013) 593–597, https://doi.org/10.1016/j.phytol.2013.07.012.
[24] I. Fonseca, I. Guarda, M. Mourato, L.L. Martins, R. Gomes, J. Matos, A. Gomes-Bispo, N.M. Bandarra, C. Cardoso, C. Afonso, Undervalued Atlantic brown seaweed species (Cystoseira abies-marina and Zonaria tournefortii): influence of treatment on their nutritional and bioactive potential and bioaccessibility, Eur. Food Res. Technol. 247 (2021) 221–232, https://doi.org/10.1007/s00217-020-03620-x.
[25] V. Gouveia, A.M.L. Seca, M.C. Barreto, D.C.G.A. Pinto, Di- and sesquiterpenoids from cystoseira genus: structure, intra-molecular transformations and biological activity, Mini Rev. Med. Chem. 13 (2013) 1150–1159, https://doi.org/10.2174/1389557511313080003.
[26] C. Bruno de Sousa, K.N. Gangadhar, J. Macridachis, M. Pavão, T.R. Morais, L. Campino, J. Varela, J.H.G. Lago, Cystoseira algae (Fucaceae): update on their chemical entities and biological activities, Tetrahedron Asymmetry 28 (2017) 1486–1505, https://doi.org/10.1016/j.tetasy.2017.10.014.
[27] J. Spavieri, A. Allmendinger, M. Kaiser, M. Itoe, G. Blunden, M. Mota, D. Tasdemir, Assessment of dual life stage antiplasmodial activity of British seaweeds, Mar. Drugs 11 (2013) 4019–4034, https://doi.org/10.3390/md11104019.
[28] J. Spavieri, A. Allmendinger, M. Kaiser, R. Casey, S. Hingley-Wilson, A. Lalvani, M. D. Guiry, G. Blunden, D. Tasdemir, Antimycobacterial, antiprotozoal and cytotoxic potential of twenty-one brown algae (phaeophyceae) from British and Irish waters, Phytother. Res. 24 (2010) 1724–1729, https://doi.org/10.1002/ptr.3208.
[29] C. Bruno de Sousa, J.H.G. Lago, J. Macridachis, M. Oliveira, L. Brito, C. Vizetto-Duarte, C. Florindo, S. Hendrickx, L. Maes, T. Morais, M. Uemi, L. Neto, L. Dionísio, S. Cortes, L. Barreira, L. Custódio, F. Alberício, L. Campino, J. Varela, Report of in vitro antileishmanial properties of Iberian macroalgae, Nat. Prod. Res 33 (2019) 1778–1782, https://doi.org/10.1080/14786419.2018.1434637.
[30] C. Bruno de Sousa, K.N. Gangadhar, T.R. Morais, G.A.A. Conserva, C. Vizetto-Duarte, H. Pereira, M.D. Laurenti, L. Campino, D. Levy, M. Uemi, L. Barreira, L. Custódio, L.F.D. Passero, J.H.G. Lago, J. Varela, Antileishmanial activity of meroditerpenoids from the macroalgae Cystoseira baccata, Exp. Parasitol. 174 (2017) 1–9, https://doi.org/10.1016/j.exppara.2017.01.002.

[31] C. Bruno de Sousa, K.N. Gangadhar, J. Macridachis, M. Pavão, T.R. Morais, L. Campino, J. Varela, J.H.G. Lago, Cystoseira algae (Fucaceae): update on their chemical entities and biological activities, Tetrahedron Asymmetry 28 (2017) 1486–1505, https://doi.org/10.1016/j.tetasy.2017.10.014.
[32] J.J. Fernández, G. Navarro, M. Norte, Novel metabolites from the brown alga Cystoseira abies-marina, Nat. Prod. Lett. 12 (1998) 285–291, https://doi.org/10.1080/10575639808048304.
[33] N. Grimblat, J.A. Gavín, A. Hernández Daranas, A.M. Sarotti, Combining the power of J coupling and dp4 analysis on stereochemical assignments: the J-DP4 methods, Org. Lett. 21 (2019) 4003–4007, https://doi.org/10.1021/acs.orglett.9b01193.
[34] N. Grimblat, M.M. Zanardi, A.M. Sarotti, Beyond DP4: an improved probability for the stereochemical assignment of isomeric compounds using quantum chemical calculations of NMR shifts, J. Org. Chem. 80 (2015) 12526–12534, https://doi.org/10.1021/acs.joc.5b02396.
[35] H.J. Domínguez, D. Cabrera-García, C. Cuadrado, A. Novelli, M.T. Fernández-Sánchez, J.J. Fernández, A.H. Daranas, Prorocentroic acid, a neuroactive super-carbon-chain compound from the dinoflagellate prorocentrum hoffmannianum, Org. Lett. 23 (2021) 13–18, https://doi.org/10.1021/acs.orglett.0c03437.
[36] J. Sosa-Rueda, V. Domínguez-Meléndez, A. Ortiz-Celiseo, F.C. López-Fentanes, C. Cuadrado, J.J. Fernández, A.H. Daranas, F. Cen-Pacheco, Squamins C–F, four cyclopeptides from the seeds of Annona globiflora, Phytochemistry 194 (2022), 112839, https://doi.org/10.1016/j.phytochem.2021.112839.
[37] C. Cuadrado, A.H. Daranas, A.M. Sarotti, May the force (Field) be with you: on the importance of conformational searches in the prediction of NMR chemical shifts, Mar. Drugs 20 (2022), https://doi.org/10.3390/md20110699.
[38] M.J. Frisch, G.W. Trucks, H.B. Schlegel, G.E. Scuseria, M.A. Robb, J.R. Cheeseman, G. Scalmani, V. Barone, B. Mennucci, G.A. Petersson, H. Nakatsuji, M., L.X. Caricato, H.P. Hratchian, A.F. Izmaylov, J. Bloino, G. Zheng, J.L. Sonnenberg, M. Hada, M. Ehara, K. Toyota, R. Fukuda, J. Hasegawa, M. Ishida, T. Nakajima, Y. Honda, O. Kitao, H. Nakai, T. Vreven, J.A. Montgomery Jr., J.E. Peralta, F. Ogliaro, M. Bearpark, J.J. Heyd, E. Brothers, K.N. Kudin, V.N. Staroverov, R. Kobayashi, J. Normand, K. Raghavachari, A. Rendell, J.C. Burant, S.S. Iyengar, J. Tomasi, M. Cossi, N. Rega, J.M. Millam, M. Klene, J.E. Knox, J.B. Cross, V. Bakken, C. Adamo, J. Jaramillo, R. Gomperts, R.E. Stratmann, O. Yazyev, A.J. Austin, R. Cammi, C. Pomelli, J.W. Ochterski, R.L. Martin, K. Morokuma, V.G. Zakrzewski, G.A. Voth, P. Salvador, J.J. Dannenberg, S. Dapprich, A.D. Daniels, O. Farkas, J.B. Foresman, J. V. Ortiz, J. Cioslowski, D.J. Fox, Gaussian 09, Revision B.01., Gaussian Inc., Wallingford. (2010).
[39] K. Wolinski, J.F. Hinton, P. Pulay, Efficient implementation of the gauge-independent atomic orbital method for NMR chemical shift calculations, J. Am. Chem. Soc. 112 (1990) 8251–8260, https://doi.org/10.1021/ja00179a005.
[40] A. González-Robles, L. Salazar-Villatoro, M. Omaña-Molina, M. Reyes-Batlle, C. M. Martín-Navarro, J. Lorenzo-Morales, Morphologica features and in vitro cytopathic effect of acanthamoeba griffini trophozoites isolated from a clinical case, J. Parasitol. Res 2014 (2014) 1–10, https://doi.org/10.1155/2014/256310.
[41] J. McBride, P.R. Ingram, F.L. Henriquez, C.W. Roberts, Development of colorimetric microtiter plate assay for assessment of antimicrobials against acanthamoeba, J. Clin. Microbiol 43 (2005) 629–634, https://doi.org/10.1128/JCM.43.2.629-634.2005.
[42] C.M. Martín-Navarro, J. Lorenzo-Morales, M.G. Cabrera-Serra, F. Rancel, N. M. Coronado-Álvarez, J.E. Piñero, B. Valladares, The potential pathogenicity of chlorhexidine-sensitive Acanthamoeba strains isolated from contact lens cases from asymptomatic individuals in Tenerife, Canary Islands, Spain, J. Med Microbiol 57 (2008) 1399–1404, https://doi.org/10.1099/jmm.0.2008/003459-0.
[43] R.L. Rodríguez-Expósito, J. Sosa-Rueda, M. Reyes-Batlle, I. Sifaoui, F. Cen-Pacheco, A.H. Daranas, A.R. Díaz-Marrero, J.E. Piñero, J.J. Fernández, J. Lorenzo-Morales, Antiamoeboid activity of squamins C–F, cyclooctapeptides from Annona globifora, Int J. Parasitol. Drugs Drug Resist 17 (2021) 67–79, https://doi.org/10.1016/j.ijpddr.2021.08.003.
[44] I. Sifaoui, P. Díaz-Rodríguez, R.L. Rodríguez-Expósito, M. Reyes-Batlle, A. López-Arencibia, L. Salazar Villatoro, I. Castelan-Ramírez, M. Omaña-Molina, A. Oliva, J. E. Piñero, J. Lorenzo-Morales, Pitavastatin loaded nanoparticles: a suitable ophthalmic treatment for Acanthamoeba Keratitis inducing cell death and autophagy in Acanthamoeba polyphaga, Eur. J. Pharm. Biopharm. 180 (2022) 11–22, https://doi.org/10.1016/j.ejpb.2022.09.020.
[45] A. González-Robles, L. Salazar-Villatoro, M. Omaña-Molina, J. Lorenzo-Morales, A. Martínez-Palomo, Acanthamoeba royreba: Morphological features and in vitro cytopathic effect, Exp. Parasitol. 133 (2013) 369–375, https://doi.org/10.1016/j.exppara.2013.01.011.
[46] C. de los, M.J. Reyes, H. Ortega, V. Zbakh, E.Zubía Motilva, Cystoseira usneoides: a brown alga rich in antioxidant and anti-inflammatory meroditerpenoids, J. Nat. Prod. 79 (2016) 395–405, https://doi.org/10.1021/acs.jnatprod.5b01067.
[47] M. Espinoza-Moraga, R. Cornejo-Morales, L.S. Santos, Synthesis and absolute configuration of (S)-(+)-chichimol ketone: the defensive secretion of walking stick Agathemera elegans, Tetrahedron Asymmetry 20 (2009) 1062–1064, https://doi.org/10.1016/j.tetasy.2009.02.030.
[48] Y. Asakawa, H. Takahashi, M. Toyota, Y. Noma, Biotransformation of monoterpenoids, (−)- and menthols, terpinolene and carvotanacetone by Aspergillus species, Phytochemistry 30 (1991) 3981–3987, https://doi.org/10.1016/0031-9422(91)83449-U.
[49] S.-W. Li, C. Cuadrado, L.-G. Yao, A.H. Daranas, Y.-W. Guo, Quantum mechanical–NMR-aided configuration and conformation of two unreported macrocycles isolated from the soft coral Lobophytum sp.: energy calculations versus coupling constants, Org. Lett. 22 (2020) 4093–4096, https://doi.org/10.1021/acs.orglett.0c01155.
[50] S.G. Smith, J.M. Goodman, Assigning stereochemistry to single diastereoisomers by GIAO NMR calculation: the DP4 probability, J. Am. Chem. Soc. 132 (2010) 12946–12959, https://doi.org/10.1021/ja105035r.
[51] A.H. Daranas, A.M. Sarotti, Are computational methods useful for structure elucidation of large and flexible molecules? Belizentrin as a case study, Org. Lett. 23 (2021) 503–507, https://doi.org/10.1021/acs.orglett.0c04016.
[52] M. Noguchi, N. Hirata, T. Tanaka, F. Suizu, H. Nakajima, J.A. Chiorini, Autophagy as a modulator of cell death machinery, Cell Death Dis. 11 (2020) 517, https://doi.org/10.1038/s41419-020-2724-5.
[53] J. Doherty, E.H. Baehrecke, Life, death and autophagy, Nat. Cell Biol. 20 (2018) 1110–1117, https://doi.org/10.1038/s41556-018-0201-5.
[54] D.R. Miller, S.D. Cramer, A. Thorburn, The interplay of autophagy and non-apoptotic cell death pathways, in: 2020: pp. 159–187. https://doi.org/10.1016/bs.ircmb.2019.12.004.
[55] D. Wu, K. Qiao, M. Feng, Y. Fu, J. Cai, Y. Deng, H. Tachibana, X. Cheng, Apoptosis of Acanthamoeba castellanii Trophozoites Induced by Oleic Acid, J. Eukaryot. Microbiol. 65 (2018) 191–199, https://doi.org/10.1111/jeu.12454.
[56] B. CHAVEZ-MUNGUIA, M. OMANA-MOLINA, M. GONZALEZ-LAZARO, A. GONZALEZ-ROBLES, P. BONILLA, A. MARTINEZ-PALOMO, Ultrastructural study of encystation and excystation in Acanthamoeba castellanii, J. Eukaryot. Microbiol 52 (2005) 153–158, https://doi.org/10.1111/j.1550-7408.2005.04-3273.x.